Atmospheric
Chemistry
and Physics
Discussions

1 # Single-particle Raman spectroscopy for studying

2 # physical and chemical processes of atmospheric particles

3 Zhancong Liang[1], Yangxi Chu[2], Masao Gen[3], Chak K. Chan[1]*

4 [1] School of Energy and Environment, City University of Hong Kong, Hong Kong, 999077, China.

5 [2] State Key Laboratory of Environmental Criteria and Risk Assessment, Chinese Research Academy of

6 Environmental Sciences, Beijing, 100012, China.

7 [3] Faculty of Frontier Engineering, Institute of Science and Engineering, Kanazawa University,

8 Kanazawa, 920-1192, Japan.

9 *Correspondence to*: Chak K. Chan (chak.k.chan@cityu.edu.hk)

10

11 **Abstract.** Atmospheric particles experience various physical and chemical processes and change their

12 properties during their lifetime. Most studies on atmospheric particles, both in laboratory and field

13 measurements, rely on analyzing an ensemble of particles. Because of different mixing state of individual

14 particles, only average properties can be obtained from studies using ensembles of particles. To better

15 understand the fate and environmental impacts of atmospheric particles, investigations on their properties

16 and processes at a single-particle level are valuable. Among a wealth of analytic techniques, single-

17 particle Raman spectroscopy provides an unambiguous characterization of individual particles under

18 atmospheric pressure in a non-destructive and in-situ manner. This paper comprehensively reviews the

19 application of such a technique in the studies of atmospheric particles, including particle hygroscopicity,

20 phase transition and separation, and solute-water interactions, particle pH, and multiphase reactions.

21 Investigations on enhanced Raman spectroscopy and bioaerosols on a single-particle basis are also

22 reviewed. For each application, we describe the principle and representative examples of studies. Finally,

23 we present our views on future directions on both technique development and further applications of

24 single-particle Raman spectroscopy in studying atmospheric particles.

25

26

27

28

29

30

31

1 Background

Atmospheric particles or aerosols have considerable effects on climate and human health.(Seinfeld and Pandis, 2016) In general, atmospheric particles can originate from a wide variety of anthropogenic and natural sources. Primary particles are emitted directly as a liquid or solid (e.g., soot particles, mineral dust), and they can also undergo atmospheric multiphase reactions. Secondary particles can also be generated by gas-to-particle conversions, such as new particle formation via nucleation and condensation.(Pöschl, 2005) During their atmospheric lifetime, both primary and secondary particles are subject to physical and chemical processes, such as partitioning and multiphase reactions. For liquid particles, gas-particle partitioning takes place to achieve thermodynamic equilibrium. For example, an increase or decrease in relative humidity (RH) would result in the uptake of the water vapor into deliquescent particles or the evaporation of particulate water to the gas phase, respectively. Multiphase reactions can be described as gas-particle partitioning accompanied by chemical reactions. Furthermore, photochemistry is an important group of multiphase reactions during the daytime. Both partitioning and chemical reactions can change the composition of the particles, altering their properties such as hygroscopicity, cloud condensation nuclei (CCN) activities, phase state, morphology, reactivity, toxicity, and finally, environmental impacts.

Physical and chemical processes of atmospheric particles have been examined by numerous experimental approaches: a flowing stream of aerosol particles in an open system, a chamber of suspending particles, a collection of deposited particles, and single particles. An aerosol flow tube is one of the most common approaches employing a flowing stream of aerosol particles. It enables real-time characterization of reaction products and particulate size under controlled conditions (e.g., RH, temperature), with instruments connected to the exit or different outlets along the flow tube reactor. Oxidation flow reactors (OFR) are analogous to the general aerosol flow tube, but photooxidants (e.g., OH radical) are introduced to examine secondary organic matter formation.(George and Abbatt, 2010;Keller and Burtscher, 2012;Kang et al., 2007;Smith et al., 2009) Typically, higher concentrations of reactive precursor gases than ambient concentrations are used in these flow systems to compensate for the relatively short residential time (e.g., seconds) of the reactants. However, such equivalency of exposure may not necessarily hold.(Lee and Chan, 2007b;Chu et al., 2019) The smog chamber enables simulations of various environmental conditions, including gas concentrations, for studying the formation and chemical

Atmospheric
Chemistry
and Physics
Discussions

62   transformation of particles. The residence time of particles can be extended to a few hours, but other

63   limitations exist, such as long response time to control/change conditions, high cost, and wall loss of

64   particles.(Kang et al., 2007) Deposited particles can be studied using a sample-loaded substrate/filter

65   placed in a flowing-gas reactor or a flow tube with its internal wall coated with particles. Environmental

66   conditions can be easily varied, and the reaction time can be very long. An in-situ analyzer for

67   spectroscopic analysis can be equipped (e.g., Raman, Fourier Transform Infrared Spectrometry (FT-IR))

68   since the particles are immobilized on a substrate/filter. However, using a large number of particles or

69   large particles is usually required to achieve sensitive detection. The influence of particle loading on the

70   reactions and chemical characterization is a challenging question. In general, these approaches produce

71   statistical results of a collection of particles. They may not truly reflect the interaction between gas and

72   particle since the composition of the individual particles may not be identical.(Ault and Axson, 2017)

73

74   Single-particle characterization has the advantage that the physical and chemical processes undertaken

75   by the particle can be unambiguously monitored. While there is a wealth of instruments for

76   comprehensively characterizing single particles, some are destructive (e.g., mass spectroscopy) or

77   operate under vacuum conditions (e.g., electron microscopy), making them unsuitable for monitoring the

78   gas-particle interaction on the same particles. Single-particle spectroscopic methods (e.g., Raman) can

79   be good alternatives, but the particles are usually supermicron and up to tens of microns. The findings

80   from particles much larger than ambient ones need to be interpreted carefully for drawing implications

81   in submicron atmospheric particles.

82

83   Despite its requirements of relatively large particles for spectroscopic signals, single-particle Raman

84   spectroscopy offers several advantages for studying the atmospheric process of aerosol particles. First of

85   all, a single particle can be unambiguously characterized *in situ* without destruction. From the Raman

86   spectra, chemical compositions of typical aerosol particles (e.g., soot, sulfate, organics, etc.) can be

87   identified by their characteristic peaks. Interactions between molecules can be inferred by peak shifts

88   and changes in peak width. Particulate properties such as the phase state and size can also be

89   characterized by coupling levitation (or isolation) technique and optical microscopy. We will elaborate

90   on the applications of these functions later.

91

92   Furthermore, Raman analysis is operated under atmospheric pressure and enables the use of atmospheric

93   relevant concentrations for a long exposure time(Lee and Chan, 2007a) to examine atmospheric gas-

94   particle interactions. Micro-Raman systems provide the spatial information of chemical species at 2-D

95   or even 3-D levels.(Tripathi et al., 2009;Batonneau et al., 2006;Offroy et al., 2015;Sobanska et al.,

96   2014;Sobanska et al., 2015;Sobanska et al., 2006;Falgayrac et al., 2018;Scolaro et al., 2009b;Ao et al.,

97   2020) Recent advances in stimulated Raman scattering by micro-Raman further improves the spatial

98   resolution from 1 μm to 350 nm and significantly shortens the scanning time from 2.5 h to 2 s.(Ao et al.,

99   2020) The disadvantage of Raman spectroscopy is that it can only detect Raman-active functional groups

100 but cannot provide information on the exact molecular structures. Sometimes, light-absorbing chemicals

101 such as HULIS or some brown carbon species may generate fluorescence, interfering with the peak

102 identification in the spectra. Therefore, single-particle Raman spectroscopy is more suited for laboratory-

103 generated particles than ambient particles. FTIR does not suffer from fluorescence since it uses a longer

104 wavelength (up to tens of μm), but the long wavelength also lowers the spectral resolution.(Ault and

105 Axson, 2017;Liu et al., 2020) Also, Raman has advantages over FTIR for water-containing samples

106 because the strong water peaks in the latter can mask the peaks from other components or even make

107 them undetectable.(Nishikida et al., 2018)

108

109 This paper will introduce the general setup of the single-particle Raman spectrometer, how single

110 particles can be characterized unambiguously, and examples of physical and chemical processes reported

111 in the literature. We focus on applications of atmospheric relevance and refer readers to other literature

112 on the principles of Raman spectroscopy and related techniques (e.g., stimulated Raman or coherent

113 Anti-stokes Raman spectroscopy) and applications with less direct atmospheric relevance (e.g.,

114 pharmaceuticals).(Tolles et al., 1977;Jones et al., 2019;Efremov et al., 2008) Finally, we will provide

115 suggestions on future directions of Raman spectroscopy for atmospheric particle studies.

116

117 **2 General set up of single-particle Raman spectroscopy**

118 **2.1 Particle isolation**

119 In general, single-particle Raman spectroscopy consists of two key components: particle isolation and

120 Raman spectroscopy, including micro-Raman and confocal Raman configurations. One of the most

121 popular approaches for single-particle isolation is particle levitation, which has been discussed in a few

122 reviews.(Reid and Mitchem, 2006;Mitchem and Reid, 2008;Krieger et al., 2012) In this paper, we will

123 briefly introduce their principles and configurations and focus on atmospheric applications. Techniques

124 for levitation of particles can be mainly divided into electrical, optical, and acoustic trapping. Another

125 approach for particle isolation is particle deposition onto substrates with Raman analyses of single

126 particles on an individual basis.

127

128 **2.1.1 Electrodynamic balance**

129 The Electrodynamic balance (EDB) has been used for studying single particles with a diameter of 1-

130 100μm since the 1980s (Davis and Ray, 1980). A particle is levitated and trapped at the null point under

131 the alternating current (AC) and direct current (DC) electric fields in the EDB. In the absence of other

132 forces, the gravitational force of the particle trapped in the EDB is equal to the balancing electrostatic

133 force, as shown in Eq. (1)

134 $$mg = nqC\frac{V_{DC}}{z} \tag{1}$$

135 where m is the mass of the particle, g is the gravitational constant, n is the number of elementary

136 charges present on the particle, q is the elementary charge, z is the distance between two electrodes

137 for the DC voltage, C is a constant dependent on the geometrical configuration of the EDB, and V_{DC}

138 is the balancing DC voltage required to levitate the particle stationary. According to Eq. (1), the mass of

139 the particle is proportional to the DC voltage needed to balance its gravitational force, assuming that the

140 charge present on the trapped particle remains constant. Hence, the relative mass change in the particle

141 undergoing any physical or chemical processing can be quantified by measuring the balancing DC

142 voltage. With a particle levitated stationary, Raman spectroscopy of the stably trapped particles can

143 provide chemical information. Coupling with mass change measurements and optical microscopy,

144 physical and chemical characterization of single particles can be in-situ monitored.

145

146 **2.1.2 Optical trapping**

147 Optical trapping utilizes the radiation pressure from a light source to balance the weight of the levitated

148 particle.(Ashkin, 1970) During optical trapping, the particle interacts with a highly focused laser beam

149 and experiences scattering and gradient forces.(Mitchem and Reid, 2008;Ashkin and Dziedzic, 1981)

150 The scattering force is proportional to the square of the induced dipoles and the intensity of the incident

151   laser beam, acting as a force along the direction of the beam propagation. In contrast, the gradient force

152   derives from the focusing of the laser beam and draws the particle towards the region with the highest

153   light intensity.(Krieger et al., 2012)

154

155   Optical levitation and optical tweezer are two typical optical-trapping techniques utilizing these two

156   forces. While optical levitation relies on the exact balance between downward gravitational force and

157   upward scattering force, optical tweezers effectively create a strong intensity gradient in three dimensions

158   by tightening the focus of the laser beam to generate amplified gradient forces. Optical tweezers provide

159   a more robust trap with the gradient force typically many orders of magnitude larger than the scattering

160   and gravitational forces, leading to 3-dimensional confinement in position with a single laser beam.

161   However, particle size changes must be accompanied by dynamic changes in the light intensity for

162   retaining the trapped particle. In principle, transparent non-absorbing particles of 1–100 μm in diameter

163   can be trapped with dynamic light intensity adjustment for droplet size changes. By configuring the

164   Bessel beam in either vertically or horizontally trapping arrangements, optical levitation and tweezer can

165   be applied for trapping submicron particles(Meresman et al., 2009). However, Raman spectroscopy

166   would require larger particles for sufficient signal-to-noise ratios. A recent study reported a

167   photochemical study of aerosol particles using an optical trap for the first time by employing a custom-

168   built photochemical levitation chamber.(Gómez Castaño et al., 2019) A sidewall of the chamber is

169   equipped with quartz windows for a UV lamp.

170

171   **2.1.3 Acoustic levitation**

172   Compared to the EDB and optical trap, acoustic levitation is less utilized in atmospheric research due to

173   the complicated acoustic streaming and the requirement for large particles (20 μm- 2 mm.).(Cohen et al.,

174   2020;Jones et al., 2021) In an acoustic levitator, high-frequency sound waves generated by a piezo-

175   electric radiator reflect from a concave-shaped reflector to generate a standing wave. The latter produces

176   acoustic radiation pressure on the particle, levitating and trapping it against the gravitational force. It has

177   been reported that a single particle can be firmly trapped by acoustic levitation under 15 h continuous

178   irradiation.(Tobon et al., 2017;Seng et al., 2018)

179

180   **2.1.4 Deposited particles**

181   In addition to single-particle levitation, deposited particles on a surface provide a convenient platform

182   for single-particle Raman spectroscopy. While levitation can trap few particles for investigation, surface-

183   based isolation affords a relatively large number of single particles, which can support further off-line

184   characterizations. However, the direct contact between particle and substrate may induce solute

185   nucleation or phase separation that causes unexpected modification in particulate morphology. Hence,

186   hydrophobic substrates are often used to study supersaturated aqueous droplets by reducing the particle

187   and substrate contact area. Investigations on photochemistry can be easily performed by coupling a

188   transparent substrate and an additional light source beneath the quartz window at a flow cell's

189   bottom.(Gen et al., 2019b;Gen et al., 2020) A single particle can be retained for an infinite time deposited,

190   facilitating studies of slow processes in the atmosphere. However, Raman scattering from the substrate

191   could also show interference.

192

193   **2.2 Raman spectroscopy**

194   A single particle Raman spectroscopy set-up generally involves a laser for excitation, followed by

195   collection optics to detect the Raman signals analyzed by a spectrometer with a monochromator and a

196   CCD detector. The Raman peak location and intensity/area provide information on the speciation and

197   abundance of specific particulate components. Appendix A summarizes the Raman peak assignment of

198   representative atmospheric species. Raman peak can also shift its location (in wavenumber) and change

199   in the full width at half-maxima (FWHM) as a response to variations of local bonding environments,

200   such as molecular interaction and phase transition. Furthermore, Raman emissions from spherical

201   particles (e.g., levitated droplets) can be complicated by resonance modes at discrete wavelengths, or so-

202   called size parameters in the spectra. These resonant modes are often called morphology-dependent

203   resonance (MDRs) or whispering gallery modes (WGMs). They can accurately determine size with a

204   resolution down to ~5 nm (corresponding to an uncertainty of ~0.058%) [39], refractive index, and even

205   shell-core morphology of the mixed organic-inorganic particles [39, 40] based on the Mie theory. Micro-

206   Raman is a combined system that uses an optical microscope for guiding the laser to analyte particles

207   and collect Raman scattering from the same microscope connected to a spectrometer. The Raman

208   scattering signal-to-noise ratio can be enhanced since the incident laser energy is focused on a small

209   volume through a high magnification (and short working distance) objective. Furthermore, 2D Raman

210   imaging is possible in studying particles in the order of tens of microns.(Eom et al., 2016;Zhao et al.,

211   2018b) Confocal Raman micro-spectroscopy eliminates the Raman scattering from volumes other than

212   the focal volume by configuring additional slits in the spectrometer. Confocal Raman provides depth

213   profiles of constituent information of the particle.(Scolaro et al., 2009a)

214

215   **3 Characterization of single particles**

216   **3.1 Hygroscopicity and phase transition**

217   Depending on the environmental RH, type of solutes, and size of the particles (Kelvin effect),

218   atmospheric particles can absorb/release an appropriate amount of water to reach equilibrium with the

219   gas phase, i.e., the partial water vapor pressure above the particle surface equals to that of the gas phase.

220   Hygroscopic properties include water uptake/evaporation and phase transition as a response to changes

221   in ambient RH. Upon water uptake/evaporation, the particle size change alters the particulate capacity in

222   scattering light, and particles can also be activated to cloud condensation nuclei.(Tang et al., 2019) In

223   this paper, we focus on subsaturated (RH <100%) environments. The phase states determine the water

224   uptake behaviors of the atmospheric particles. They can be generally divided into liquid (i.e., aqueous),

225   crystalline, and amorphous (e.g., ultra-viscous, gel, rubber, glasses). Both crystalline and amorphous

226   particles are solids, but only the latter can absorb water reversibly, while the former shows hysteresis in

227   water uptake. At increasing RH, water uptake increases the aerosol liquid water (ALW) content of

228   deliquescent/amorphous particles and their size and ability to scatter light. A recent study showed that

229   the poor visibility during haze in the North China Plain is positively correlated to the ALW(Wu et al.,

230   2018). When crystalline particles are exposed to increasing RH, they will initially adsorb a small amount

231   of water on its surface, the so-called surface adsorbed water (SAW), and then uptake a significant amount

232   of water vapor abruptly to become aqueous droplets at the deliquescence RH (DRH). The DRH is the

233   RH at which a droplet attains the saturated salt concentration, ignoring the influence of the Kelvin effect,

234   which is often the case for single-particle Raman analysis (particle size > 10 μm). At decreasing RH, a

235   droplet loses water to become supersaturated and finally may effloresce to form crystalline particles at

236   the efflorescence RH (ERH). Typical inorganic atmospheric components of $(NH_4)_2SO_4$, NH_4NO_3 and

237   NaCl deliquesce at ~80%, ~62% and ~75% RH but effloresce at 34-48%, 0-30% and 39-54%,

238   respectively. Many studies show that nitrates and some organics do not effloresce even at low RH. (e.g.,

239   below 5%)(Yeung and Chan, 2010;Mikhailov et al., 2009) In general, organics with high solubility (e.g.,

240   malonic acid) tend to remain a supersaturated liquid state or amorphous state at low RH.(Krieger et al.,

241 2012) Unlike DRH, which is thermodynamically well defined, ERH is a stochastic property that relates

242 to the kinetics of nucleation and presence of impurities. It has been reported that sucrose crystals

243 deliquesce at 85.6%RH upon humidification, but the aqueous droplets turn into a glassy amorphous state

244 upon drying instead of forming crystallized solids.(Zobrist et al., 2011) Using EDB and optical trap

245 experiments, hygroscopic changes and phase transition RH values that involve rapid changes in mass or

246 size can be measured by the balancing voltage and light scattering, respectively. The growth factor (GF)

247 in terms of mass or size ratios as a function of water activity or RH, DRH, and ERH can be easily

248 determined by changes in mass/size and the light scattering pattern.(Mitchem et al., 2006;Chan et al.,

249 2005)

250

251 While GF, DRH, and ERH measurements are readily made for mixed particles using EDB and optical

252 traps, the formation of mixed-phase particles before full deliquescence is more complicated. For example,

253 unlike the corresponding single inorganic salts, NaCl-malonic acid and $(NH_4)_2SO_4$-malonic acid mixed

254 particles absorb a significant amount of water before their DRH since malonic acid absorbs water

255 reversibly without crystallization.(Lee et al., 2008a) However, this stepwise water uptake and phase

256 transition behaviors could not be explained by EDB/optical levitation due to the lack of chemical

257 characterization. Raman spectroscopy offers complementary information on the water uptake behaviors

258 and phase states of Raman active species. For example, the water-to- solute ratio (WSR) as a function of

259 ambient RH can be easily determined from the integrated peak area ratio of the water v(O–H) to that of

260 the solute (e.g., sulfate, nitrate) after proper calibration. Also, the full width at half maxima (FWHM) of

261 the characteristic peaks is sensitive to the phase state of the solute. In general, a species in the liquid

262 phase has a larger FWHM than in the solid phase because the less compact molecular arrangement allows

263 minor variations in vibration. In Fig. 1a,b, as the RH decreased to 39.5% for ammonium sulfate (AS)

264 and 19% for ammonium nitrate (AN), crystallization can be inferred by the red-shift and decrease in

265 FWHM of sulfate and nitrate peaks, and the disappearance of water peak. On this basis, the mixed-phase

266 particle prior to full deliquescence can be characterized by FWHM of different Raman-active

267 components. For instance, an increased FWHM of nitrate peak was found (~730 cm^{-1}) at ~67% RH,

268 followed by an increased FWHM of sulfate peak (~450 cm^{-1}) at ~76 RH% for mixed-phase AS-AN

269 particles when RH increased (Fig. 1c,d). These changes indicate that AN deliquesced before AS did upon

270 humidification, and the mixed-phase AS-AN particle was composed mainly of aqueous AN and

271 crystalline AS. The accuracy of single-particle Raman spectroscopy in determining hygroscopicity has

272 been verified by thermodynamic models such as E-AIM and UNIFAC.(Peng et al., 2001;Yeung and Chan,

273 2010)

274

275 **3.2 Solid-phase transition**

276 In addition to liquid-solid phase changes, transitions can occur between solid phases, from a metastable

277 one to a stable one at a specific temperature. Many organics are known to form polymorphs, defined as

278 solids with the same chemical composition but distinctive properties such as thermal stability and

279 solubility due to different structures.(Krieger et al., 2012) Different polymorphs of the same compound

280 can exhibit other Raman characteristics, which can identify different solid states and their transition. For

281 example, crystalline glutaric acid (GA) particles could exist as the metastable α-form and the

282 thermodynamically stable β-form at room temperature, and α-form GA tends to transfer into β-form.

283 Using EDB-Raman, Chan et al. coated GA on AS particles by coagulation of small GA particles formed

284 by nucleation. Raman spectra showed the existence of α-form GA in the freshly coated particles, but

285 then β-form was detected after a deliquescence - crystallization cycle.(Chan et al., 2006) Ling and Chan

286 reported the formation of the α-form GA solid in a freshly crystallized GA-AS particle. The α-form GA

287 solid gradually transformed to the β-form at 60% RH in 3 h at room temperature.(Ling and Chan, 2008)

288 Furthermore, Yeung et al. examined the effects of polymorphism on the hygroscopic properties of GA

289 particles using Micro-Raman(Yeung et al., 2010). By evaporation at room temperature, α-form and β-

290 form solid particles were formed ($\alpha:\beta \approx 5:1$). It was observed that the α-form deliquesced at 85-86%

291 RH, whereas the β-form deliquesced at 90% RH. Furthermore, the α-form is transformed to the β-

292 form at 86% RH instead of achieving full deliquescence (Fig. 2). This solid phase transition behavior

293 was used to explain the discrepancies of DRH values of glutaric acid particles reported based on different

294 literature measurements.(Cruz and Pandis, 2000;Peng et al., 2001;Zardini et al., 2008;Parsons et al.,

295 2004;Treuel et al., 2009;Choi and Chan, 2002) Polymorphism also exists in atmospheric relevant

296 inorganics. For example, AN can exist in five stable polymorphic forms with distinct Raman spectra,

297 depending on the temperature. In atmospheric research, very little attention has been paid to the solid

298 phase transitions of AN because phase IV AN particle is stable over a wide range of tropospheric

299 temperatures ($-17°C \sim 32°C$).(Wu et al., 2007) Nevertheless, Wu and co-workers reported that the

300 KNO$_3$/AN mixed particles undergo the IV-III transition under ambient temperatures at a relatively high

Atmospheric
Chemistry
and Physics
Discussions
Open Access
EGU

301   mass percentage of KNO_3(≥7.4 wt%), or even crystallize directly in phase III from droplets with a further

302   increase in the mass percentage of KNO_3.(Wu and Chan, 2008)

303

304   Another typical solid phase transition is between stable/metastable double salts.   Like

305   metastable/stable polymorphs, metastable double salts show Raman characteristics different from stable

306   ones, likely due to specific molecular interactions. Ling et al. observed the double-salt 3AN·AS, not

307   predicted from thermodynamics, in the freshly crystallized mixed single particles of AN and AS using

308   single-particle Raman spectroscopy. The existence of double salts indicates that AN and AS likely

309   crystalized simultaneously. The degree of metastability could depend upon the crystallization processes

310   of the particles. Besides, it takes several hours to more than a day, depending on RH, for a freshly

311   crystallized metastable AS-AN double salt particle to reach its stable form, suggesting a high possibility

312   that metastable solids persist in the atmosphere when the ambient RH is sufficiently low. The AN-AS

313   double salts were recently reported in ambient particles during haze events in Beijing with a considerable

314   amount.(Sun et al., 2019b)

315

316   **3.3 Molecular interactions between particulate water and solutes**

317   In general, characterizations on phase transitions relies on the sensitivity of Raman spectroscopy in

318   probing the bonding environment of components in the particles. Raman can also characterize the

319   interactions between the solutes and particulate water, such as hydrogen/ionic bonding. For example, the

320   Raman shift of strongly hydrogen-bonded water (~3500 cm^{-1}) is generally higher than that of water

321   monomers (~3300 cm^{-1}).(Zhang and Chan, 2003) At low RH, the elevated concentration of electrolytes

322   leads to more significant disruption of the hydrogen bonding environment of the water molecules,

323   resulting in a shift of OH stretching peak at 3480cm^{-1} to higher frequencies. In contrast, the low-

324   frequency shoulder at 3290 cm^{-1} diminishes. Thus, the shape of water peaks in Raman spectra can reflect

325   the ionic strength of the particle, which is an essential parameter for aerosol chemistry.(Mekic et al.,

326   2020;Mitchem et al., 2006) The sensitive shift of water peak has also been used in studying ice nucleation

327   properties such as depositional freezing(Wise et al., 2012;Wise et al., 2010) and immersing

328   freezing(Knopf et al., 2003;Knopf et al., 2002). Specifically, while liquid water peaks are usually located

329   at ~3400cm^{-1} with a shoulder at a lower wavenumber, a sharp peak at ~3150 cm^{-1} with shoulder peaks at

330   ~3200cm^{-1} appears as water is frozen.(Mael et al., 2019;Schill et al., 2014) Besides, ionic bonding of

Atmospheric
Chemistry
and Physics
Discussions

Open Access

EGU

331   inorganic salts (e.g., SO_4^{2-}, NO_3^-) can also be reflected by their Raman characteristics; and many of them

332   have been further supported by theoretical calculations.(Yu et al., 2012;Zhu et al., 2018;Wang et al.,

333   2015b) For example, Zhang et al. observed a blue shift of sulfate and nitrate Raman peaks and an increase

334   in FWHM when the molar water to the solute ratio (WSR) in $MgSO_4$ and $Mg(NO_3)_2$ particles decreases

335   to less than six, the number of hydration of Mg^{2+} ions.(Zhang and Chan, 2000;Zhang et al., 2004) These

336   observations were attributed to direct contacting ion pairs formed between Mg^{2+} and anions, without

337   water molecules between the ions. Besides, single-particle Raman spectroscopic analysis can reveal the

338   structural heterogeneity of droplets. Raman imaging suggested that the NO_3^- to Mg^{2+} ratio of the contact

339   ion pairs increases but the H_2O to Mg^{2+} ratio decreases as the surface of a highly supersaturated droplet

340   is approached.(Zhang et al., 2004) Yeung et al. reported that though no crystallization was shown by

341   glyoxylic acid particle even at 0% RH, a new C=O peak at ~1820cm^{-1} appeared together with the aqueous

342   C=O peak at 1735 cm^{-1}, possibly indicating the presence of anhydrate.(Yeung and Chan, 2010)

343

344   **3.4 Liquid-liquid phase separation**

345   As mentioned above, partial crystallization can lead to a separation of solid and liquid mixed phases.

346   Separation of two or even more liquid phases, namely liquid-liquid phase separation (LLPS), is also

347   possible. LLPS can be triggered by the interactions between inorganic, organic solutes and particulate

348   water in mixed particles containing organics and inorganics.(You et al., 2012) This phenomenon is

349   mainly attributed to the low solubility of some non-polar or weakly polar organics, especially in the

350   presence of inorganic salt, which may further decrease the solubilities of organics as the salting-out

351   effects.(Setschenow, 1889) Single-particle (micro-) Raman spectroscopy has been used for probing

352   LLPS via spatial scanning (micro-Raman), optical imaging (micro-Raman), Raman imaging, and

353   whisper gallery modes (WGMs).(Bertram et al., 2011;Song et al., 2012a;Buajarern et al., 2007a) Spatial

354   scanning records distinct micro-Raman spectra at different locations of the particle for indicating

355   LLPS(Bertram et al., 2011). However, this approach requires accurate focusing of the laser onto different

356   targeted phases, which can be difficult when phases are separated into small inclusions.(Buajarern et al.,

357   2007b) Alternatively, optical microscopy can directly indicate LLPS by the contrasting colors on

358   appearance, based on the different refractive indices of materials in different phases. The RH for first

359   observing the separated inclusions in the image is defined as separation RH (SRH).(You et al., 2012;Song

360   et al., 2012b;You et al., 2014;You et al., 2013;Song et al., 2013) Using optical microscopy, SRH of a

361 wide range of mixed particles has been correlated with the O:C ratio, organic to inorganic ratio, particle

362 size, and temperature.(Bertram et al., 2011;You et al., 2014) Another approach for identifying LLPS is

363 Raman imaging of the whole particle. Typical Raman measurements bin the vertical pixels of a CCD to

364 enhance the signal to noise ratio while the horizontal pixels represent wave number after chromatic

365 dispersion by a grating. For this imaging of the whole particle, binning is not used and the CCD detector

366 captures a one-dimensional image of the particle after the monochromator. The vertical pixels register

367 the vertical profile of the Raman scattering (e.g., edge to center to edge) of the particles. Chu et al.

368 reported that the core-shell phase separation in a mixed sucrose-ammonium sulfate particle with a sucrose

369 molar fraction of 50% at <5% RH, but not at 70%RH.(Chu and Chan, 2017a) As shown in Fig. 3a, b, the

370 accumulated C-H signal at two sides indicates the presence of an organic-rich coating and an organic-

371 deficient core. In contrast, the even distribution of the C-H signal in Fig. 3c suggests that the particle is

372 likely homogeneous. Additionally, WGMs have also been utilized to infer the occurrence of LLPS and

373 the specific particle morphologies. For example, different resonance structures can appear in the Raman

374 spectra when core-shell or engulfed phase separation occurs.(Buajarern et al., 2007a, b;Kwamena et al.,

375 2010;Song et al., 2013) Sharps peaks generated by WGMs in spectra can be found if the spatial

376 distribution of particulate species is symmetric, such as those in core-shell separated and homogeneously

377 mixed particles though the number, location, and intensity of WGMs peaks are different. In contrast, the

378 engulfed phase-separated particles do not show any WGMs peaks.

379

380 **3.5 Determination of pH**

381 The pH, defined as the activity of proton in aerosol particles, can also be inferred from Raman spectra

382 based on the intensity of the conjugate acid/base ion pairs. Sulfate/bisulfate has been used most frequently.

383 The pH can be determined by substituting the conjugate ion pair concentrations and its dissociation

384 coefficient into Henderson-Hasselbalch (H-H),(Radić and Prkić, 2012) Debye-Hückel theory, and

385 specific ion interaction theory equations, respectively.(Ciavatta, 1980;Craig et al., 2017;Coddens et al.,

386 2019;Craig et al., 2018;Rindelaub et al., 2016) The latter two are more suitable to supersaturated particles

387 since non-ideality has been considered. Rindelaub et al. reported direct measurements of pH in individual

388 deposited particles according to sulfate/bisulfate peaks in Raman spectra, and its variation with

389 RH.(Rindelaub et al., 2016) Craig et al. extended this approach to a range of atmospherically relevant

390 inorganic and organic acid-base equilibria systems covering a wide range of pH (-1~10).(Craig et al.,

391   2017) To eliminate the artifact of contacts between the particle and the substrate, Coddens et al.

392   determined the pH of trapped particles via titration by coalescence of droplets containing strong

393   acids.(Coddens et al., 2019) Boyer et al. further utilized the WGMs for determining the solute

394   concentration in real-time and achieve uncertainties in pH measurements of picoliter droplets ranging

395   from ±0.03 to 0.06 pH units.(Boyer et al., 2020)

396

397   **4 Multiphase reactions**

398   In Section 3, applications of characterizing single particles have been reviewed. This section mainly

399   focuses on the "processes" occurring on single particles.   Taking water-solute interactions as an example,

400   hygroscopicity describes the ability of solutes to absorb water upon equilibrium at fixed RH. Water

401   uptake is a dynamic process, although it is generally too quick to be a limiting step in most atmospheric

402   applications. However, in some viscous matrixes, the water uptake rate could be reduced by orders of

403   magnitude due to the limited diffusion. Taking advantage of the different Raman characteristics of D_2O

404   and H_2O, Davies and Wilson measured the diffusion coefficients of water molecules in trapped viscous

405   particles by monitoring the isotopic exchange rate using Raman spectroscopy.(Davies and Wilson, 2016)

406   Determination of kinetic parameters of non-reactive processes such as partitioning coefficient, diffusion

407   coefficient, and mass accommodation coefficient has been reviewed in another paper(Krieger et al.,

408   2012). Hence, applications on probing multiphase reactions using single-particle Raman spectroscopy

409   will be the focus below.

410

411   **4.1 Multiphase formation of secondary inorganic aerosols (SIA)**

412   Particulate sulfate and nitrate are two major secondary inorganic aerosols (SIA). They have dominant

413   Raman peaks at ~980 cm^{-1} and ~1046 cm^{-1}, respectively. Probing multiphase formation of sulfate by

414   single-particle Raman spectroscopy was first employed by Davis and co-workers for absorption of SO_2

415   by alkali-metal hydroxides particles.(Aardahl and Davis, 1996) In atmospheric applications, particulate

416   sulfate formation has been a debating topic since the currently proposed pathways, including O_3, OH

417   radical, NO_2, H_2O_2, and transition metal ions (TMI), cannot entirely account for the high concentration

418   of sulfate observed in haze events such as those in the North China Plain (NCP).(Cheng et al., 2016)

419   Using single-particle micro-Raman spectroscopy, Chan and his group reported that oxidants including

420   NO_2, N(III), OH radicals, etc., generated from particulate nitrate photolysis could effectively oxidize SO_2

421   to sulfate.(Gen et al., 2019b;Gen et al., 2019c;Zhang et al., 2020;Zheng et al., 2020b) Clear increase of

422   the sulfate peak signal was identified in Raman spectra of UV irradiated nitrate particle (Fig. 4). Later,

423   they also reported sulfate formation by multiphase oxidation of SO_2 during $FeCl_3$ photolysis.(Gen et al.,

424   2020) The formation of nitrate has also been investigated.

425

426   Zangmeister and Pemberton performed kinetic analysis on the reactions between deposited NaCl

427   particles and gaseous HNO_3 based on the increase of the nitrate peak.(Zangmeister and Pemberton, 2001)

428   Tang et al. coupled optical levitation with Raman spectroscopy to investigate N_2O_5 uptake on SiO_2

429   particle as a function of RH and found that particulate nitrate formation increased as RH increased. They

430   conclude that the water content affects the partitioning of HNO_3 between the gas phase and condensed

431   phases (i.e., adsorbed phase and aqueous phase). More surface adsorbed water layers block the reactive

432   sites for N_2O_5 uptake but promote HNO_3 dissolution. Scolaro et al. studied the three-dimensional

433   evolution of the NaCl(100) surface during its reaction with NO_2 as a function of RH, using confocal

434   Raman imaging combined with non-contact atomic force microscopy (AFM).(Scolaro et al., 2009a) At

435   0% RH, a $NaNO_3$ monolayer capping the NaCl(100) surface formed. $NaNO_3$ tetrahedral crystals (<0.5

436   μm) formed at 45% RH, and supermicron $NaNO_3$ rhombohedral plates were obtained under the H_2O

437   multilayer regime (45%<RH<75%). At RH>80%, both crystalline and aqueous NO_3^- were found.

438   Reactions were accelerated in the presence of water vapor due to the formation of reactive HNO_3 by NO_2

439   hydrolysis. Ault et al. reported that individual nascent sea spray aerosol particles showed different

440   reactivity toward HNO_3 and N_2O_5, likely due to compositional heterogeneity. After the same exposure

441   of gaseous reactants, some particles showed intense $v(NO_3^-)$ peak, whereas $v(C-H)$ is still the dominant

442   mode in some other particles.(Ault et al., 2014)

443

444   There are also investigations on the simultaneous formation of particulate sulfate and nitrate. Zhao et al.

445   reported a multi-step reaction mechanism of oxidation of SO_2 by NO_2 on deposited $CaCO_3$

446   particles.(Zhao et al., 2018a)Further, Yu and Zhao et al. reported that the uptake coefficient of SO_2 on

447    $CaCO_3$ particles in the presence of O_2/NO_2 mixture was much higher than that without O_2.(Yu et al., 2018)

448   The synergy of NO_2 and O_2, which involved mechanisms such as chain reactions, resulted in much faster

449   sulfate formation than the sum of the reaction rates with NO_2 and with O_2 alone. These reports show the

450   usefulness of single-particle Raman spectroscopy in studying the multiphase formation of particulate

Atmospheric
Chemistry
and Physics
Discussions

Open Access

EGU

451   sulfate and nitrate. It is worth mentioning that degradation of organo-sulfate has been proposed to

452   produce particulate inorganic sulfate recently(Xu et al., 2020b) and organo-sulfate functional groups are

453   also Raman-active. (Bondy et al., 2018) Raman spectroscopy may find applications in the study of

454   organo-sulfates.

455

456   **4.2 Multiphase formation of SOA**

457   Most of the organic compounds are Raman-active though some of them may not have strong signals.

458   Some generate fluorescence in general orders of magnitude stronger than Raman emissions, masking

459   useful Raman features of particles. The characteristic peaks of a single organic compound are generally

460   more than that of an inorganic one due to its complex molecular vibration modes, and the reaction

461   products may further complicate spectra analysis. Therefore, investigation on the multiphase formation

462   of SOA by Raman spectroscopy is limited. However, though identifying the molecular nature of the

463   products is difficult, single-particle Raman spectroscopy can provide useful information during

464   secondary organic aerosol (SOA) formation. For example, Lee et al. observed a gradually elevating

465   baseline in Raman spectra during acid-catalyzed octanol uptake by levitated sulfuric acid particles at 10%

466   RH but not at 50% RH.(Lee et al., 2008b) Though the speciation of products could not be resolved, the

467   increasing fluorescence is evident, attributable to the formed SOA in the particles. Using an EDB, Chan

468   and Chan examined the dependence of nonanal on the presence of hydrophilic and hydrophobic organics

469   in acidic mixed organic-sulfuric acid particles. The presence of hydrophobic organic materials (oleic acid

470   and its reaction products with sulfuric acid) enhanced SOA formation by reactive uptake of nonanal,

471   likely through an enhanced dissolution of nonanal in the particles.(Chan and Chan, 2011) In contrast,

472   levoglucosan, a hydrophilic organic, did not increase the uptake coefficient of nonanal. It is suggested

473   that acid-catalyzed reactive uptake should be examined with the explicit consideration of the role of

474   particle-phase organics that are either initially present or accumulated as a reaction product. Using micro-

475   Raman, Olson et al. investigated the uptake of isoprene epoxydiol (IEPOX) by α-pinene SOA/toluene

476   SOA-coated AS particles.(Olson et al., 2019) Before the uptake, both coated AS particles show core-

477   shell morphology. v(N-H) and $v(SO_4^{2-})$ were found at ~3200cm^{-1} and ~976cm^{-1} in the particle core, while

478   strong v(C-H) at 2800-3000cm^{-1} and other moderate/weak stretches of C-H were found in the shell region.

479   After the uptake, v(C-H) and v(RO−SO$_3$) were found in the particle core, indicating SOA formation,

480   such as organo-sulfate. No organo-sulfate was detected in shell regions of both types of particles,

Atmospheric
Chemistry
and Physics
Discussions
Open Access
EGU

481   although decreases of ν(C-H) peak were apparent. Generally, Raman analysis is useful for kinetic

482   analysis of reactions (e.g., measuring uptake coefficients), but it is challenging to reveal complicated

483   mechanisms due to the limited molecular identification. For better examining the reaction mechanism,

484   deposited particles can be extracted for off-line analysis using mass spectrometry (MS)(Chan et al.,

485   2013;Li et al., 2008), although the simultaneous mass and phase state information would not be available.

486

487   **4.3 Multiphase oxidation of organic aerosol particles**

488   In addition to reactive uptake of SOA precursors, single-particle Raman spectroscopy has also been used

489   to explore the uptake of oxidants by organic aerosol particles. So far, the reported studies are limited to

490   ozonolysis. Raman spectroscopy is well suited in ozonolysis studies because the C=C bonds and the

491   peroxide groups are Raman-active, and ozonolysis does not generate strongly fluorescent products.

492   Using single-particle Raman spectroscopy, Lee and Chan performed in-situ observations of the particle

493   mass, hygroscopicity, morphology of the oleic acid(Lee and Chan, 2007a), linolenic acid, and linoleic

494   acid particles(Lee and Chan, 2007b) during ozonolysis. They found that low ozone concentration

495   (∼200−250 ppb) with a longer exposure period (20 h) favors autoxidation to form C=C−C=C groups;

496   but an extremely high ozone concentration (∼10 ppm) at shorter exposure time (2 h) tends to form

497   carboxylic acids (C=O), secondary ozonide (O-O), hydroxyalkyl hydroperoxide (O-H), etc.(Qiu et al.,

498   2020;Enami and Colussi, 2017) Chu et al. further examined the interchangeability between ozone

499   concentration and exposure time by studying ozonolysis of linoleic acid particles in a broader range of

500   experimental conditions. They found the interchangeability holds at ozone exposure ≤ 500 ppb h and [O_3]

501   ≤ 100 ppb for the formation of autoxidation products containing conjugated diene structures but does not

502   hold for the decay of parent linoleic acid or at higher [O_3].(Chu et al., 2019) These results indicate that

503   extrapolating experimental results of the ozonolysis under high [O_3] conditions to ambient levels should

504   be carried out with caution. Single-particle Raman spectroscopy also enables us to infer the volatilization

505   of some ozonolysis products. For example, Lee and Chan found that the mass of oleic acid particles was

506   observed to decrease with time while that of linoleic acid and linolenic acid increased on the contrary,

507   which could be potentially explained by the different volatility of the ozonolysis products.(Lee and Chan,

508   2007b) King et al. reported an optical tweezers study of ozonolysis of oleic acid and synthetic seawater

509   droplets. They found clear Raman signatures indicating nonanoic acid and nonanal production, followed

510   by their gradual disappearance, which is also likely due to the volatilization.(King et al., 2004)

511   Furthermore, Dennis-Smither et al. used optical tweezers to study the oxidation of oleic acid droplets

512   containing an inorganic seed with a time-resolution of 1 s to resolve the reactive loss of ozone and the

513   evaporative loss of products. The oleic acid ozonolysis was completed in ~3000 s, but the decrease of

514   droplet volume still lasts for an additional ~5000 s due to the slow volatilization of the products .(Dennis-

515   Smither et al., 2012)

516

517   Chan and Chan studied the roles of the phase state and water content in the ozonolysis of maleic acid

518   (MA) and AS mixed particles. Aqueous MA was found to be more reactive toward ozone than crystalline

519   MA. Interestingly, they also found that higher water content favors more efficient ozonolysis, although

520   the concentration of MA is accordingly lower.(Chan and Chan, 2012) Furthermore, ozonolysis of

521   optically trapped bioaerosol particles has also been reported. In general, lipids and proteins show distinct

522   v(C-H) peaks at 2855 cm^{-1} and 2928 cm^{-1}, respectively.(Kline and Treado, 1997;Rygula et al.,

523   2013;Czamara et al., 2015) The ratio of these peaks can be thus used for inferring the different

524   susceptibilities of lipids and proteins during ozonolysis oxidation.(Gong et al., 2019) The products

525   derived from oxidations such as carbonyls (C=O; ~1700 cm^{-1})(Lee and Chan, 2007b) and oligomer of

526   cysteine (C-S; ~662cm^{-1})(Kampf et al., 2015;Movasaghi et al., 2007) are also detected.

527

528   There are also studies exploring other organic surrogates of atmospheric aerosol with more complicated

529   structures. For example, King et al. measured the uptake coefficients of ozone on fumarate and benzoate

530   droplets (as a proxy of HULIS-containing aerosol) and α-pinene droplets (a proxy of biogenic organic

531   aerosol).(King et al., 2008) Different reaction products such as carbonate were identified in Raman

532   spectra, though the chemical characterization is not comprehensive due to their volatility and the

533   detection limits. The reaction of α-pinene in the droplet phase was more than one order faster than in

534   bulk aqueous solutions, likely due to more effective diffusion of ozone in the gas phase and more efficient

535   mass accommodation at the air-droplet interface.(King et al., 2008)

536

537   **4.4 Amine/Ammonia reactions**

538   Ammonia and amines are the most abundant alkaline gases in the atmosphere. They play a significant

539   role in new particle formation and buffering aerosol pH by neutralization of acidic particles.(Zhang et

540   al., 2015;Kerminen et al., 2018;Kirkby et al., 2011;Almeida et al., 2013;Zheng et al., 2020a) There are

Atmospheric
Chemistry
and Physics
Discussions

541   three types of reactions involving ammonia and amines: (1) Neutralization reaction between acidic

542   particles and ammonia/amines; (2) Displacement of ammonia by amines from ammonium salt particles

543   and vice versa from aminium salt particles; (3) Reactions between ammonia/amines and dissolved di-

544   carbonyls or between gaseous di-carbonyls and ammonium/aminium salt particles, both would result in

545   the formation of colored compounds (i.e., Brown carbon; BrC).

546

547   Based on the strong vibration signal of the C-H bond ($\sim 2900 cm^{-1}$, sharp peak) from amine/aminium salts

548   and the N-H bond (~ 2800-$3300\ cm^{-1}$, broad peak), the uptake of amine and ammonia can be easily studied

549   using single-particle Raman spectroscopy. Sauerwein and Chan explored the role of phase state in

550   simultaneous uptake of ammonia and dimethylamine (DMA) by acidic particles (e.g., sulfuric acid and

551   oxalic acid).(Sauerwein and Chan, 2017) Anhydrous acidic particles were inert and took up DMA and

552   ammonia presumably by adsorption only. The uptake rates of DMA and ammonia by aqueous acidic

553   droplets were found comparable initially, but once the droplets were neutralized, the stronger base DMA

554   displaced some of the particulate ammonium. On the other hand, if crystallization took place during the

555   uptake, DMA uptake was inhibited, but continuous ammonia uptake gradually displaced the particle

556   DMA ions.

557

558   Chan and Chan reported that the exchange reactions of ammonia/amine vapors in aqueous particles were

559   reversible, and the exchange rates of aqueous particles were, in general, higher than those of their

560   corresponding solid counterparts. Compared with crystalline solids (e.g., methylammonium sulfate),

561   amorphous solid (e.g., diethylammonium sulfate) was found with a higher exchange rate, likely due to

562   the less compact molecular structure.(Chan and Chan, 2013) Chu and Chan further examined the effect

563   of a hydrophilic viscous organic surrogate and a hydrophobic organic coating on DMA uptake by AS.

564   Both the viscous materials and the fresh and aged organic coating retarded DMA uptake by mass transfer

565   limitation.(Chu and Chan, 2017a;Chu and Chan, 2017b) The uptake of DMA by crystalized AS particles

566   at 10-30% RH resulted in the deliquescence of the particles, likely due to the presence of surface adsorbed

567   water (SAW) that promoted the dissolution of DMA. Once dimethylaminium sulfate is formed, it absorbs

568   more water since it is more hygroscopic than AS and further promoted DMA uptake.(Chu and Chan,

569   2017a) As crystalline solids are generally considered inert towards reactions, this finding indicates that

570   SAW on crystals can serve as a medium to facilitate gas uptake.

Atmospheric
Chemistry
and Physics
Discussions

Open Access

EGU

571

572   BrC has attracted increasing attention due to its atmospheric abundance and capacity in regulating

573   radiative balance.(Laskin et al., 2015) The reactions between dicarbonyls and ammonium/aminium-

574   containing salt particles can form BrC. Gen et al. investigated the multiphase uptake of glyoxal by

575   ammonium salt-containing particles using Micro-Raman spectroscopy. They found a gradual elevation

576   of the baseline, which was attributed to the formation of a fluorescent BrC (i.e., 2,2′-biimidazole, BI),

577   based on off-line analysis by UV-VIS spectroscopy and fluorescence spectroscopy.(Gen et al., 2018) The

578   reduction in ALW at low RH increases the glyoxal uptake rate via the enhanced "salting-in" effect and

579   the BI formation rate by facilitating dehydration reactions. Mabato et al. examined glyoxal uptake by

580   methylaminium salt-containing particle. Although the "salting-in" effect was also found in

581   methylaminium salt-containing particles, enhanced BI formation was not observed, likely due to the

582   higher hygroscopicity of methylaminium salt (i.e., higher ALW content) than ammonium salt.(Mabato et

583   al., 2019)

584

585   **4.5 Photochemistry of aerosol particles**

586   A particular type of aerosol particle reaction that deserves special attention is photochemical reactions,

587   which can be initiated by irradiation of the particles. Nitrate can be photolyzed under atmospheric

588   irradiation ($\lambda > 290nm$). Nitrate photolysis proceeds via three channels: one produces NO_2 and OH

589   radicals, another produces NO_2^- and $O(^3P)$ and the last generates $ONOO^-$. The third channel's quantum

590   yield is considered negligible compared with the former two since ONOO is unstable. It has been

591   reported that NO_2^- and ONOO- peaks increased, but NO_3^- peaks decreased in the Raman spectra of

592   acoustically levitated nitrate particles irradiated by UV.(Tobon et al., 2017) NO_2 does not have a large

593   absorption cross-section, but it may be hydrolyzed into NO_2^-.(Tobon et al., 2017;Seng et al., 2018;Gómez

594   Castaño et al., 2019) Most nitrate photolysis products are oxidants, so their ability to initiate oxidation

595   reactions has also been explored(Gen et al., 2019b;Gen et al., 2019c;Zhang et al., 2020). The production

596   of sulfate via nitrate photolysis was discussed earlier. Recently, Zhang et al. reported a prominent formate

597   production by glyoxal oxidation during particulate nitrate photolysis, instead of the more commonly

598   found oxalic acids oligomers in the oxidation of glyoxal in bulk solutions.(Zhang et al., 2021)

599   Furthermore, Liang et al. reported nitrate photolysis in particles containing sucrose, which was used as

600   a surrogate for atmospheric viscous organics. They found that the viscosity of the particle did not reduce

601 the nitrate photolysis rate, but it limited the diffusion of gaseous products (e.g., NOx, NOy) from nitrate

602 photolysis. At a high sucrose fraction and 30%RH, the production of these gaseous products and the

603 particles' viscosity transformed the droplets into "hollow and enlarged" semi-solid particles.(Liang et al.,

604 2021)

605

606 Size dependence of nitrate photochemistry has been recently reported, based on single-particle Raman

607 spectroscopy. Tobon et al. studied photolysis acoustically levitated nitrate particles (40~80μm) at 254nm

608 UV radiation. No change in Raman spectra for 2 h. In contrast, smaller particles (5~8μm) trapped

609 optically yielded various Raman peaks of nitrate photolysis products.(Gómez Castaño et al., 2019;Tobon

610 et al., 2017) The slow photolysis in the larger nitrate particles was attributed to the self-inhibited surface

611 process. Additionally, an uneven distribution of NO_2^- inside the smaller particle was also observed

612 through Raman mapping.(Gómez Castaño et al., 2019) Organics in the aerosol particle may also

613 decompose under light. For example, Farmentier et al. reported photodegradation of optically trapped

614 oleic acid droplets under 532 nm and 660 nm irradiation, likely initiated by photosensitization. However,

615 they cautioned that degradation loss of optically trapped particles might be artifacts. The photo-decay of

616 light-absorbing particulate matters is also of great interest in understanding their fate in the atmosphere.

617 However, there are very limited studies of atmospheric photochemical reactions using Raman

618 spectroscopy, partly because of the need for complementary chemical speciation for detailed mechanistic

619 studies.

620

621 **5 Enhanced Raman spectroscopy**

622 Though Raman has been used to study physical and chemical processes of atmospheric particles, most

623 of the studies used large particles (dozens of microns) and focused on lab-generated particles with a few

624 representative components. That is primarily because of the intrinsic diffraction limitation of Raman

625 measurements that the laser beam cannot be effectively focused to a spot smaller than its wavelength and

626 thus limits the detection of particles to larger than 1 micron or so. Fluorescence can also be a complication

627 in some chemical systems.

628

629 Various methods have been developed to improve the Raman signal-to-noise ratios and the spatial

630 resolution in other research fields such as material science and biology. Surface-enhanced Raman

631   spectroscopy (SERS) and Tip-enhanced Raman spectroscopy (TERS) have been recently employed in

632   atmospheric research. SERS and TERS enhance Raman emissions by the localized surface plasmon

633   resonances using noble metal nanoparticles (NPs) to provide "hot spots" near the contacting sites between

634   the analyte and NPs.(Ault and Axson, 2017) According to the SERS electromagnetic (EM) enhancement

635   theory, the relationship between the SERS intensity (I) and the local EM strength (E) follows $I \propto |E|^4$.

636   The relationship between E and the distance between NPs and analytes (D) is described as $E \propto$

637   (1/D).(Zhou et al., 2015) Hence, maximizing E and minimizing D without inducing significant

638   perturbation to the sample is the primary goal. In addition to this physical enhancement based on the

639   electromagnetic field, Raman signals can also be enhanced chemically. Specifically, molecular/ionic

640   species can attach to the surface of NPs, distorting the molecular structure and increasing the absorption

641   cross-section. Consequently, the Raman signal of an adsorbed species can be enhanced, potentially

642   accompanied by a peak shift.(Gen and Chan, 2017;Craig et al., 2015)

643

644   SERS enables the measurements of single particles smaller than 1 micron. Craig et al. found that the

645   signals from individual submicron (down to 0.6 μm) particles could be effectively detected with intensity

646   enhancement.(Craig et al., 2015) Furthermore, Tirella et al. extended the SERS detection to the

647   accumulation mode (800~150 nm) particles(Tirella et al., 2018). Sun et al. reported a size-resolved

648   (covering both coarse mode and accumulation mode) SERS characterization study of atmospheric

649   particles sampled during haze events.(Sun et al., 2019a;Sun et al., 2019b) More recently, Kunihisa et al.

650   reported sensitive SERS measurement of Aiken mode particles (<100nm) by combining a condensational

651   growth tube sampler (CGT) and a SERS substrate for directly sampling.(Kunihisa et al., 2020) The wide

652   analytical range of particle size enables SERS to be a potentially powerful tool in studying ambient

653   particulate matters.(Vejpongsa et al., 2017;Steer et al., 2016;Chen et al., 2021)

654

655   Some species including components of microorganisms(Tahir et al., 2020), microplastics(Xu et al.,

656   2020a), crystalline silica(Zheng et al., 2018), the fine structure of organics(Craig et al., 2015;Gen et al.,

657   2018;Fu et al., 2017), and even some Raman-active inorganic salts at very low concentration(Saniel et

658   al., 2019) are invisible in normal Raman due to their weak Raman-activities. However, they could be

659   detected with a SERS substrate. The sensitive detection by SERS can provide valuable insight into

660   particle transformations and emission sources.(Vejpongsa et al., 2017;Ghosal and Wall, 2019;Lee et al.,

661 2019) However, the enhancement factor of SERS is not constant. It strongly depends on the distribution

662 and quantity of noble metal NPs and the hotspots over the substrate, making quantitative analysis difficult.

663 Many attempts have been made to explore preferable and tunable substrate for generalizable atmospheric

664 particle detection,(Cheng et al., 2021;Xu et al., 2020a) but still more progresses are needed in the future.

665

666 The most common SERS application uses particles deposited on SERS substrates, relying on the "hot

667 spot" locating beneath the analyte particles. Recently, some studies create innovative interactions

668 between particulate analytes and SERS NPs to enhance SERS detections. Wei et al. used 4-

669 mercaptobenzoic acid-functionalized AuNPs as pH nanoprobes and internal SERS substrate and found

670 the existence of a stable pH gradient inside aqueous particles.(Wei et al., 2018a) Hence, the assumption

671 of homogeneous mixing might not always be correct, and pH predictions by thermodynamic model might

672 underestimate the acidity of interfacial layers of particles, which is crucial for multiphase uptake or

673 surface reactions. As a further investigation of the SERS pH nanoprobe, Huang et al. reported that the

674 pH distribution inside aerosol particles is affected by the internal distribution of ions, which may depend

675 on the ionic speciation. While sodium tends to reside in the bulk of the particle, leading to a high centroid

676 pH, ammonium distributes more evenly due to its increased surface propensity.(Huang et al., 2020)

677

678 Gen et al. developed an electrospray system (ES-SERS) to deposit SERS NPs onto the surface of the

679 analyte particle and found that this technique can selectively enhance the peak intensity of the species

680 located at surface layers such as surface adsorbed water(Gen and Chan, 2017) and organic coatings(Gen

681 et al., 2019a). In a typical micro-Raman set-up, the objective is above the analyte particle. When the

682 analyte particle is deposited on the SERS substrate, the SERS hot spots are located beneath the particle.

683 In other words, upon laser irradiation from the top, the photons generated by excitation need to pass

684 through the particle with a refractive index greater than air, which would scatter or absorb light and thus

685 reduces the signals received by the Raman microscope. In contrast, ES-SERS hot spots are created on

686 the surface of the particle using electrospray. This configuration reduces the loss of photons and affords

687 greater enhancement in the Raman intensity. (Fig. 5) Besides, as the SERS effect is much more prominent

688 near the hot spots (i.e., small D), the location of the hot spots determines where will be probed in SERS

689 spectra. Therefore, while typical SERS substrate collects enhanced Raman signals from the substrate-

690 particle interface, the ES-SERS can provide information from the gas-particle interface, where many

691   atmospheric multiphase processes occur. Sivaprakasam et al. reported real-time SERS measurements of

692   electrostatically trapped particles containing analyte molecules and NPs as internally mixed liquid

693   particles or coating on solid particles.(Sivaprakasam et al., 2017;Sivaprakasam and Hart, 2021) The

694   interaction between NPs and analyte increased due to more contact areas than that between an aerosol

695   particle and a substrate.

696

697   Similarly, TERS can produce enhanced Raman signals even from particles in the nucleation mode. TERS

698   is a combination of atomic force microscope (AFM) and Raman spectrometer. In general, AFM

699   determines the topography of a single deposited particle by detecting the interaction force between the

700   AFM tip and the surface of the analytes. In a typical TERS set-up, the AFM tip is coated with noble

701   metal particles. An enhanced Raman signal is generated when the tip is interacting with analytes under

702   laser excitation.(Rodriguez et al., 2015) The lack of chemical information of AFM is complemented by

703   SERS. Thus, TERS enables simultaneous characterization of particulate topography and surface species

704   of submicron particles at a high spatial resolution.(Ofner et al., 2016) TERS also has the potential for

705   quantitative analysis since the quantity and configuration of hotspots on the tip are constant.

706

707   **6 Bioaerosols**

708   Bioaerosols have attracted increasing attention worldwide dramatically due to the COVID-19 epidemic.

709   Studies using normal Raman/SERS for off-line detection of biological samples(Félix-Rivera and

710   Hernández-Rivera, 2012;Mosier-Boss, 2017), real-time sensing of bioaerosol(Huffman et al., 2020) have

711   been reviewed in detail elsewhere. Bioaerosols have various Raman active components such as

712   phosphate lipid (δ (=C-H), ~1268cm^{-1}; v(C-H), ~2855cm^{-1}), protein (amides bands, ~1260cm^{-1},

713   ~1600cm^{-1}, ~1660cm^{-1}; C-C backbone stretching in β-sheet proteins, ~983cm^{-1}; v(C-H), ~2928cm^{-1}) and

714   nucleic acids (e.g., adenine, ~735cm^{-1}), etc.(Socrates, 2004;Talari et al., 2015;Rygula et al., 2013)

715   However, Raman signals from bioaerosol particles are generally weak. To amplify the signals, bioaerosol

716   particles are trapped or deposited onto a substrate for longer integration time.(Tripathi et al., 2009;Laucks

717   et al., 2000;Sengupta et al., 2005;Wang et al., 2015a;Ai et al., 2020;Redding et al., 2015) Using a higher

718   energy laser can also enhance Raman intensity, but it may cause damage to bioaerosol (e.g.,

719   fragmentation).(Gong et al., 2017) On this basis, SERS is more suitable than normal Raman spectroscopy.

720   SERS can also quench the fluorescence generated by biomolecules such as tryptophan and

721   tyrosine.(Gong et al., 2017)

722

723   In general, there are two strategies of single-particle SERS of bioaerosols: (1) directly sampling

724   bioaerosols on a SERS substrate; (2) moving mixed colloids of SERS NPs and bioaerosols onto a glass

725   substrate, followed by drying. While the former is more convenient without complex pretreatments(Tahir

726   et al., 2020), the latter enables flexible modification of NPs properties. For example, functionalized

727   surface of NPs with tag molecules (e.g., antibody), so-called label-based SERS(Liu et al., 2010), were

728   used for detecting specific biomaterials with high reproducibility. Label-free SERS refers to that without

729   tag molecules, such as Au@Ag. In general, by simply mixing, NPs distribute on biomaterials without

730   specific interactions, and the SERS reproducibility is limited. However, by coating AgNPs on the cell

731   wall of bacteria,(Zhou et al., 2014a;Zhou et al., 2015) SERS enhancement was ~30-folds reproducibly

732   higher than simply mixed colloid−bacterial suspension. Furthermore, the discrimination of live and dead

733   bacteria was possible. NPs can be directly formed inside some specific bacteria via bio-reduction for

734   probing the intercellular structure.(Jarvis et al., 2008) Overall, SERS can be an innovative tool in

735   bioaerosol characterization, but the antibacterial effect of NPs and heat effect due to excitation laser

736   should be considered.(Mosier-Boss, 2017) More examples of bioaerosol detection can be found in a

737   recent review.(Liu et al., 2017)

738

739   **7 Future directions**

740   This review paper has shown examples of single-particle Raman spectroscopy in studying atmospheric

741   processes. Overall, the water content, phase state, morphology, and chemical composition of single

742   particles during physical and chemical processes at controlled RH can be monitored in situ.

743   Hygroscopicity and phase behaviors covering a wide range of RH after these processes can also be

744   comprehensively assessed by performing evaporation-humidification cycle measurements.(Chan et al.,

745   2006;Chan and Chan, 2007;Chen et al., 2020;Liu et al., 2008) Although fluorescence may exist in some

746   particles, it could be potentially reduced or even eliminated by (1) using longer excitation wavelengths

747   (e.g., 785 and 1064 nm); (2) employing SERS/TERS; (3) photo-bleaching of fluorescent substances

748   under UV-VIS illumination.(Gong et al., 2017) There are many other innovative studies built on trapping,

749   manipulating, and observing multi-particles via Raman(Davies, 2019;Mitchem and Reid, 2008), such as

750   measuring viscosity and diffusion coefficient(Power et al., 2013), probing reaction(Aardahl,

Atmospheric
Chemistry
and Physics
Discussions

751   1998;Rkiouak et al., 2014) and phase transition(Richards et al., 2020). Based on these functions and

752   research progresses, we would like to provide the following suggestions on future directions:

753

754   ● **Hyphenated single-particle Raman spectroscopy.** Raman spectroscopy is non-destructive, so

755   incorporating other spectroscopic techniques for characterizing the same particle is possible.

756   Vibrational sum frequency generation spectroscopy (SFG), Fourier transform infrared spectroscopy

757   (FT-IR), and fluorescence spectroscopy, which are also non-destructive, could be complementary

758   to Raman in probing chemical composition of single particle. Recently, novel combination of EDB

759   and mass spectrometry was reported, which can directly introduce the trapped particle for mass

760   spectrometry analysis.(Birdsall et al., 2018;Willis et al., 2020;Jacobs et al., 2017) Adaption of this

761   technique with Raman to form an EDB – Raman system with subsequent MS analysis is relatively

762   straight forward. For optical properties, UV/Vis spectroscopy could be a promising choice.(Jones

763   et al., 2021) While general laser-based MDR can easily bleach light-absorbing molecules, a recent

764   study reported that MDR modes under broad band excitation can measure refractive index (RI) of

765   light-sensitive samples.(Price et al., 2020) Such MDR measuremens can complement in-situ Raman

766   spectroscopy for chemical characterization. Additionally, SERS/TERS are emerging useful

767   approaches, but current SERS/TERS methods for atmospheric research mainly use bare NPs. The

768   direct contact of NPs to analyte molecules can potentially induce chemical enhancement, which

769   could complicate the identification of the phase transition and functional groups.(Gen and Chan,

770   2017;Craig et al., 2015) To remove the chemical enhancement, future studies on chemically inert

771   NPs such as shell-isolated nanoparticle-enhanced Raman spectroscopy (SHINERS) are

772   suggested.(Li et al., 2010;Anema et al., 2011)

773

774   ● **Multiphase reaction studies based on single-particle Raman spectroscopy.** Single-particle

775   Raman spectroscopy enables investigations of various atmospheric reactions, including those in

776   surface adsorbed water for solids, mixed-phase particles (solid, aqueous, organic), supersaturated

777   droplets, atmospheric aging of bioaerosols and ultrafast reactions. For solid particles (e.g.,

778   crystalline, mineral dust), multiphase reactions can be "mediated" by surface adsorbed water layers

779   and may result in phase transition, turning the particle into liquid for further reactions.(Kuwata and

780   Martin, 2012;Chu and Chan, 2017a;Zhao et al., 2018a;Yu et al., 2018;Gen et al., 2019a) Probing

Atmospheric
Chemistry
and Physics
Discussions
Open Access
EGU

781 heterogenous reactions on the particle surface is possible via ES-SERS, TERS, and normal Raman

782 imaging. As particle constituents can be unevenly distributed (e.g., in LLPS) within a single particle,

783 chemistry may not be the same between the bulk and the surface layers.(Wei et al., 2018b;Huang et

784 al., 2020;Olson et al., 2019;Lam et al., 2021;Qiu et al., 2019) The studies of the atmospheric

785 processing of pre-existing particles to form secondary aerosols can be further extended to the aging

786 of bioaerosols.(Gong et al., 2019) Using pulse laser for excitation, time-resolved resonance Raman

787 spectroscopy (TR3) can be a promising tool in probing short-lived reactive intermediates (e.g.,

788 triplet state molecules). In particular, it helps deepen our understanding in ultrafast reactions or

789 initiation steps of typical reactions.(Sahoo et al., 2011;Collins et al., 2018)

790

791 ● **Particle size and temperature effects.** Many publications report single-particle Raman

792 spectroscopy studies under different environmental conditions, including RH and gas concentration,

793 etc. However, how experimental conditions such as temperature and particle size affect kinetics and

794 products in multiphase reactions remains ambiguous. For example, various pathways and kinetic

795 parameters have been proposed to explain particulate sulfate formation in winter haze events in

796 northern China.(Chan and Yao, 2008;Su et al., 2020) However, most studies are based on

797 experimental results at room temperature or 298K. Further exploration with respect to the effect of

798 low temperature on the properties of the particles and multiphase sulfate chemistry is still warranted.

799 Employing a temperature-controlled cold plate flow cell - Raman system for deposited single

800 particles(Roy et al., 2020;Mael et al., 2019;Wheeler et al., 2015), investigations of temperature-

801 dependent reaction kinetics can be easily achieved. Temperature control in a small levitation

802 chamber is also more convenient than in a flow tube or smog chamber. To date, almost all single-

803 particle Raman studies involve supermicron particles. While equilibrium measurements are not

804 sensitive to size (assuming the Kelvin effect is considered), kinetic analysis is often size-dependent.

805 Hence, uptake coefficients for multiphase reactions are usually reported and are restricted to

806 experimental conditions that gas and liquid phase transport are not the rate-limiting step. The size

807 detection limit of single-particle Raman spectroscopy can be extended to sub-10 micrometer with

808 high sensitiveity using high-energy excitation laser and tighter optical focusing. The effect of

809 temperature and particle size on multiphase chemistry should be further investigated using long

810 integration time, novel optical configuration (e.g., confocal micro-Raman), and SERS/TERS, etc.

Atmospheric
Chemistry
and Physics
Discussions

811   Although it is challenging to study single submicron particles by Raman spectroscopy regularly,

812   Raman characterization of a collection of single submicron particles is feasible.

813

814   *Competing interests.* The authors declare that they have no conflict of interest.

815

821

References

823   Aardahl, C. L., and Davis, E. J. P. B.: Gas/Aerosol Chemical Reactions in the NaOH-SO2-H2O System,

824   Applied Spectroscopy, 50, 71-77, 1996.

825   Aardahl, C. L. W. J. F. D. E. J.: Raman Analysis of Chemical Reactions Resulting from the Collision of

826   Micrometer-Sized Particles, Applied Spectroscopy, 52, 47-53, 1998.

827   Ai, Y., Alali, H., Pan, Y.-L., Videen, G., and Wang, C.: Single-particle optical-trapping raman

828   spectroscopy for the detection and identification of aerosolized airborne biological particles,

829   Measurement Science and Technology, 10.1088/1361-6501/abd5f1, 2020.

830   Almeida, J., Schobesberger, S., Kürten, A., Ortega, I. K., Kupiainen-Määttä, O., Praplan, A. P., Adamov,

831   A., Amorim, A., Bianchi, F., and Breitenlechner, M.: Molecular understanding of sulphuric

832   acid–amine particle nucleation in the atmosphere, Nature, 502, 359-363, 2013.

833   Anema, J. R., Li, J.-F., Yang, Z.-L., Ren, B., and Tian, Z.-Q.: Shell-Isolated Nanoparticle-Enhanced

834   Raman Spectroscopy: Expanding the Versatility of Surface-Enhanced Raman Scattering,

835   Annual Review of Analytical Chemistry, 4, 129-150, 10.1146/annurev.anchem.111808.073632,

836   2011.

837   Ao, J., Feng, Y., Wu, S., Wang, T., Ling, J., Zhang, L., and Ji, M.: Rapid, 3D Chemical Profiling of

838   Individual Atmospheric Aerosols with Stimulated Raman Scattering Microscopy, Small

839   Methods, 4, 1900600, https://doi.org/10.1002/smtd.201900600, 2020.

840   Ashkin, A.: Acceleration and Trapping of Particles by Radiation Pressure, Physical Review Letters, 24,

841   156-159, 10.1103/PhysRevLett.24.156, 1970.

842   Ashkin, A., and Dziedzic, J.: Observation of optical resonances of dielectric spheres by light scattering,

843   Appl. Opt., 20, 1803-1814, 1981.

844   Ault, A. P., Guasco, T. L., Baltrusaitis, J., Ryder, O. S., Trueblood, J. V., Collins, D. B., Ruppel, M. J.,

845   Cuadra-Rodriguez, L. A., Prather, K. A., and Grassian, V. H.: Heterogeneous Reactivity of

846   Nitric Acid with Nascent Sea Spray Aerosol: Large Differences Observed between and within

847   Individual Particles, The Journal of Physical Chemistry Letters, 5, 2493-2500,

848   10.1021/jz5008802, 2014.

849   Ault, A. P., and Axson, J. L.: Atmospheric Aerosol Chemistry: Spectroscopic and Microscopic Advances,

850   Analytical Chemistry, 89, 430-452, 10.1021/acs.analchem.6b04670, 2017.

851   Batonneau, Y., Sobanska, S., Laureyns, J., and Bremard, C.: Confocal Microprobe Raman Imaging of

852   Urban Tropospheric Aerosol Particles, Environmental Science & Technology, 40, 1300-1306,

853   10.1021/es051294x, 2006.

854   Bertram, A., Martin, S., Hanna, S., Smith, M., Bodsworth, A., Chen, Q., Kuwata, M., Liu, A., You, Y.,

855   and Zorn, S.: Predicting the relative humidities of liquid-liquid phase separation, efflorescence,

856   and deliquescence of mixed particles of ammonium sulfate, organic material, and water using

857   the organic-to-sulfate mass ratio of the particle and the oxygen-to-carbon elemental ratio of the

858   organic component, Atmospheric Chemistry & Physics, 11, 2011.

859   Birdsall, A. W., Krieger, U. K., and Keutsch, F. N.: Electrodynamic balance–mass spectrometry of single

860   particles as a new platform for atmospheric chemistry research, Atmospheric Measurement

861   Techniques, 11, 33-47, 2018.

862   Bondy, A. L., Craig, R. L., Zhang, Z., Gold, A., Surratt, J. D., and Ault, A. P.: Isoprene-Derived

863   Organosulfates: Vibrational Mode Analysis by Raman Spectroscopy, Acidity-Dependent

864   Spectral Modes, and Observation in Individual Atmospheric Particles, The Journal of Physical

865   Chemistry A, 122, 303-315, 10.1021/acs.jpca.7b10587, 2018.

866   Boyer, H. C., Gorkowski, K., and Sullivan, R. C.: In Situ pH Measurements of Individual Levitated

867   Microdroplets Using Aerosol Optical Tweezers, Analytical Chemistry, 92, 1089-1096,

868   10.1021/acs.analchem.9b04152, 2020.

869   Buajarern, J., Mitchem, L., and Reid, J. P.: Characterizing Multiphase Organic/Inorganic/Aqueous

870   Aerosol Droplets, The Journal of Physical Chemistry A, 111, 9054-9061, 10.1021/jp074366a,

871   2007a.

872   Buajarern, J., Mitchem, L., and Reid, J. P.: Characterizing the Formation of Organic Layers on the

873   Surface of Inorganic/Aqueous Aerosols by Raman Spectroscopy, The Journal of Physical

874   Chemistry A, 111, 11852-11859, 10.1021/jp075021v, 2007b.

875   Carey, D. M., and Korenowski, G. M.: Measurement of the Raman spectrum of liquid water, The Journal

876   of chemical physics, 108, 2669-2675, 1998.

877   Chan, C. K., and Yao, X.: Air pollution in mega cities in China, Atmospheric Environment, 42, 1-42,

878   10.1016/j.atmosenv.2007.09.003, 2008.

879   Chan, K. M., Huang, D. D., Li, Y. J., Chan, M. N., Seinfeld, J. H., and Chan, C. K.: Oligomeric products

880   and formation mechanisms from acid-catalyzed reactions of methyl vinyl ketone on acidic

881   sulfate particles, Journal of Atmospheric Chemistry, 70, 1-18, 2013.

882   Chan, L. P., and Chan, C. K.: Enhanced Reactive Uptake of Nonanal by Acidic Aerosols in the Presence

883   of   Particle-Phase   Organics,   Aerosol   Science   and   Technology,   45,   872-883,

884   10.1080/02786826.2011.567314, 2011.

885   Chan, L. P., and Chan, C. K.: Roles of the Phase State and Water Content in Ozonolysis of Internal

886   Mixtures of Maleic Acid and Ammonium Sulfate Particles, Aerosol Science and Technology,

887   46, 781-793, 10.1080/02786826.2012.665514, 2012.

888   Chan, L. P., and Chan, C. K.: Role of the aerosol phase state in ammonia/amines exchange reactions,

889   Environmental science & technology, 47, 5755-5762, 2013.

890   Chan, M. N., Choi, M. Y., Ng, N. L., and Chan, C. K.: Hygroscopicity of Water-Soluble Organic

891   Compounds in Atmospheric Aerosols: Amino Acids and Biomass Burning Derived Organic

892   Species, Environmental Science & Technology, 39, 1555-1562, 10.1021/es049584l, 2005.

893   Chan, M. N., Lee, A. K., and Chan, C. K.: Responses of ammonium sulfate particles coated with glutaric

894   acid to cyclic changes in relative humidity: Hygroscopicity and Raman characterization,

895   Environmental science & technology, 40, 6983-6989, 2006.

896   Chan, M. N., and Chan, C. K.: Mass transfer effects on the hygroscopic growth of ammonium sulfate

897   particles   with   a   water-insoluble   coating,   Atmospheric   Environment,   41,   4423-4433,

898   https://doi.org/10.1016/j.atmosenv.2007.01.047, 2007.

899   Chen, H., Duan, F., Du, J., Yin, R., Zhu, L., Dong, J., He, K., Sun, Z., and Wang, S.: Surface-enhanced

900   Raman scattering for mixing state characterization of individual fine particles during a haze

901   episode in Beijing, China, Journal of Environmental Sciences, 104, 216-224,
902   https://doi.org/10.1016/j.jes.2020.12.008, 2021.
903   Chen, X., Chu, Y., Lee, A. K., Gen, M., Kasthuriarachchi, N. Y., Chan, C. K., and Li, Y. J.: Relative
904   humidity history affects hygroscopicity of mixed particles of glyoxal and reduced nitrogenous
905   species, Environmental science & technology, 54, 7097-7106, 2020.
906   Cheng, H., Dong, X., Yang, Y., Feng, Y., Wang, T., Tahir, M. A., Zhang, L., and Fu, H.: Au nanoring
907   arrays as surface enhanced Raman spectroscopy substrate for chemical component study of
908   individual atmospheric aerosol particle, Journal of Environmental Sciences, 100, 11-17,
909   https://doi.org/10.1016/j.jes.2020.07.003, 2021.
910   Cheng, Y., Zheng, G., Wei, C., Mu, Q., Zheng, B., Wang, Z., Gao, M., Zhang, Q., He, K., Carmichael,
911   G., Pöschl, U., and Su, H.: Reactive nitrogen chemistry in aerosol water as a source of sulfate
912   during haze events in China, Science Advances, 2, e1601530, 10.1126/sciadv.1601530, 2016.
913   Choi, M. Y., and Chan, C. K.: The Effects of Organic Species on the Hygroscopic Behaviors of Inorganic
914   Aerosols, Environmental Science & Technology, 36, 2422-2428, 10.1021/es0113293, 2002.
915   Chu, Y., and Chan, C. K.: Reactive Uptake of Dimethylamine by Ammonium Sulfate and Ammonium
916   Sulfate–Sucrose Mixed Particles, The Journal of Physical Chemistry A, 121, 206-215,
917   10.1021/acs.jpca.6b10692, 2017a.
918   Chu, Y., and Chan, C. K.: Role of oleic acid coating in the heterogeneous uptake of dimethylamine by
919   ammonium sulfate particles, Aerosol Science and Technology, 51, 988-997,
920   10.1080/02786826.2017.1323072, 2017b.
921   Chu, Y., Cheng, T. F., Gen, M., Chan, C. K., Lee, A. K. Y., and Chan, M. N.: Effect of Ozone
922   Concentration and Relative Humidity on the Heterogeneous Oxidation of Linoleic Acid
923   Particles by Ozone: An Insight into the Interchangeability of Ozone Concentration and Time,
924   ACS Earth and Space Chemistry, 3, 779-788, 10.1021/acsearthspacechem.9b00002, 2019.
925   Ciavatta, L.: The specific interaction theory in evaluating ionic equilibria, Ann. Chim.(Rome), 70, 551,
926   1980.
927   Coddens, E. M., Angle, K. J., and Grassian, V. H.: Titration of Aerosol pH through Droplet Coalescence,
928   J Phys Chem Lett, 10, 4476-4483, 10.1021/acs.jpclett.9b00757, 2019.
929   Cohen, L., Quant, M. I., and Donaldson, D. J.: Real-Time Measurements of pH Changes in Single,
930   Acoustically Levitated Droplets Due to Atmospheric Multiphase Chemistry, ACS Earth and

931   Space Chemistry, 4, 854-861, 10.1021/acsearthspacechem.0c00041, 2020.

932   Collins, D. B., Hems, R. F., Zhou, S., Wang, C., Grignon, E., Alavy, M., Siegel, J. A., and Abbatt, J. P.

933   D.: Evidence for Gas-Surface Equilibrium Control of Indoor Nitrous Acid, Environ Sci Technol,

934   52, 12419-12427, 10.1021/acs.est.8b04512, 2018.

935   Craig, R. L., Bondy, A. L., and Ault, A. P.: Surface Enhanced Raman Spectroscopy Enables Observations

936   of Previously Undetectable Secondary Organic Aerosol Components at the Individual Particle

937   Level, Analytical Chemistry, 87, 7510-7514, 10.1021/acs.analchem.5b01507, 2015.

938   Craig, R. L., Nandy, L., Axson, J. L., Dutcher, C. S., and Ault, A. P.: Spectroscopic Determination of

939   Aerosol pH from Acid–Base Equilibria in Inorganic, Organic, and Mixed Systems, The Journal

940   of Physical Chemistry A, 121, 5690-5699, 10.1021/acs.jpca.7b05261, 2017.

941   Craig, R. L., Peterson, P. K., Nandy, L., Lei, Z., Hossain, M. A., Camarena, S., Dodson, R. A., Cook, R.

942   D., Dutcher, C. S., and Ault, A. P.: Direct Determination of Aerosol pH: Size-Resolved

943   Measurements of Submicrometer and Supermicrometer Aqueous Particles, Analytical

944   Chemistry, 90, 11232-11239, 10.1021/acs.analchem.8b00586, 2018.

945   Cruz, C. N., and Pandis, S. N.: Deliquescence and Hygroscopic Growth of Mixed Inorganic−Organic

946   Atmospheric   Aerosol,   Environmental   Science   &   Technology,   34,   4313-4319,

947   10.1021/es9907109, 2000.

948   Czamara, K., Majzner, K., Pacia, M. Z., Kochan, K., Kaczor, A., and Baranska, M.: Raman spectroscopy

949   of lipids: a review, Journal of Raman Spectroscopy, 46, 4-20, 2015.

950   Davies, J. F., and Wilson, K. R.: Raman Spectroscopy of Isotopic Water Diffusion in Ultraviscous, Glassy,

951   and Gel States in Aerosol by Use of Optical Tweezers, Analytical Chemistry, 88, 2361-2366,

952   10.1021/acs.analchem.5b04315, 2016.

953   Davies, J. F.: Mass, charge, and radius of droplets in a linear quadrupole electrodynamic balance, Aerosol

954   Science and Technology, 53, 309-320, 10.1080/02786826.2018.1559921, 2019.

955   Davis, E. J., and Ray, A.: Single aerosol particle size and mass measurements using an electrodynamic

956   balance, Journal of Colloid and Interface Science, 75, 566-576, 1980.

957   Dennis-Smither, B. J., Hanford, K. L., Kwamena, N.-O. A., Miles, R. E. H., and Reid, J. P.: Phase,

958   Morphology, and Hygroscopicity of Mixed Oleic Acid/Sodium Chloride/Water Aerosol

959   Particles before and after Ozonolysis, The Journal of Physical Chemistry A, 116, 6159-6168,

960   10.1021/jp211429f, 2012.

961   Efremov, E. V., Ariese, F., and Gooijer, C.: Achievements in resonance Raman spectroscopy: Review of
962   a technique with a distinct analytical chemistry potential, Analytica chimica acta, 606, 119-134,
963   2008.

964   Enami, S., and Colussi, A. J.: Criegee Chemistry on Aqueous Organic Surfaces, The Journal of Physical
965   Chemistry Letters, 8, 1615-1623, 10.1021/acs.jpclett.7b00434, 2017.

966   Eom, H.-J., Gupta, D., Cho, H.-R., Hwang, H. J., Hur, S. D., Gim, Y., and Ro, C.-U.: Single-particle
967   investigation of summertime and wintertime Antarctic sea spray aerosols using low-Z particle
968   EPMA, Raman microspectrometry, and ATR-FTIR imaging techniques, Atmospheric
969   Chemistry and Physics, 16, 13823-13836, 2016.

970   Falgayrac, G., Siepka, D., Stefaniak, E. A., Penel, G., and Sobanska, S.: Influence of collecting substrate
971   on the Raman imaging of micron-sized particles, Analytica Chimica Acta, 1014, 41-49,
972   https://doi.org/10.1016/j.aca.2018.02.015, 2018.

973   Félix-Rivera, H., and Hernández-Rivera, S. P.: Raman Spectroscopy Techniques for the Detection of
974   Biological Samples in Suspensions and as Aerosol Particles: A Review, Sensing and Imaging:
975   An International Journal, 13, 1-25, 10.1007/s11220-011-0067-0, 2012.

976   Fu, Y., Kuppe, C., Valev, V. K., Fu, H., Zhang, L., and Chen, J.: Surface-Enhanced Raman Spectroscopy:
977   A Facile and Rapid Method for the Chemical Component Study of Individual Atmospheric
978   Aerosol, Environmental Science & Technology, 51, 6260-6267, 10.1021/acs.est.6b05910, 2017.

979   Gen, M., and Chan, C. K.: Electrospray surface-enhanced Raman spectroscopy (ES-SERS) for probing
980   surface chemical compositions of atmospherically relevant particles, Atmospheric Chemistry &
981   Physics, 17, 2017.

982   Gen, M., Huang, D. D., and Chan, C. K.: Reactive uptake of glyoxal by ammonium-containing salt
983   particles as a function of relative humidity, Environmental science & technology, 52, 6903-6911,
984   2018.

985   Gen, M., Kunihisa, R., Matsuki, A., and Chan, C. K.: Electrospray surface-enhanced Raman
986   spectroscopy (ES-SERS) for studying organic coatings of atmospheric aerosol particles,
987   Aerosol Science and Technology, 53, 760-770, 10.1080/02786826.2019.1597964, 2019a.

988   Gen, M., Zhang, R., Huang, D. D., Li, Y., and Chan, C. K.: Heterogeneous SO2 Oxidation in Sulfate
989   Formation by Photolysis of Particulate Nitrate, Environmental Science & Technology Letters,
990   6, 86-91, 10.1021/acs.estlett.8b00681, 2019b.

991   Gen, M., Zhang, R., Huang, D. D., Li, Y., and Chan, C. K.: Heterogeneous Oxidation of SO2 in Sulfate
992   Production during Nitrate Photolysis at 300 nm: Effect of pH, Relative Humidity, Irradiation
993   Intensity, and the Presence of Organic Compounds, Environ Sci Technol, 53, 8757-8766,
994   10.1021/acs.est.9b01623, 2019c.

995   Gen, M., Zhang, R., Li, Y., and Chan, C. K.: Multiphase Photochemistry of Iron-Chloride Containing
996   Particles as a Source of Aqueous Chlorine Radicals and Its Effect on Sulfate Production,
997   Environmental Science & Technology, 54, 9862-9871, 10.1021/acs.est.0c01540, 2020.

998   George, I. J., and Abbatt, J. P.: Heterogeneous oxidation of atmospheric aerosol particles by gas-phase
999   radicals, Nat Chem, 2, 713-722, 10.1038/nchem.806, 2010.

1000   Ghosal, S., and Wall, S.: Identifying regional soil as the potential source of PM2.5 particulate matter on
1001   air filters collected in Imperial Valley, California – A Raman micro-spectroscopy study,
1002   Environmental Pollution, 253, 181-189, https://doi.org/10.1016/j.envpol.2019.07.004, 2019.

1003   Gómez Castaño, J. A., Boussekey, L., Verwaerde, J. P., Moreau, M., and Tobón, Y. A.: Enhancing Double-
1004   Beam Laser Tweezers Raman Spectroscopy (LTRS) for the Photochemical Study of Individual
1005   Airborne Microdroplets, Molecules, 24, 3325, 2019.

1006   Gong, Z., Pan, Y.-L., Videen, G., and Wang, C.: The temporal evolution process from fluorescence
1007   bleaching to clean Raman spectra of single solid particles optically trapped in air, Chemical
1008   Physics Letters, 689, 100-104, https://doi.org/10.1016/j.cplett.2017.09.064, 2017.

1009   Gong, Z., Pan, Y.-L., Videen, G., and Wang, C.: Chemical reactions of single optically trapped
1010   bioaerosols in a controlled environment, Aerosol Science and Technology, 53, 853-859,
1011   10.1080/02786826.2019.1621984, 2019.

1012   Huang, Q., Wei, H., Marr, L. C., and Vikesland, P. J.: Direct Quantification of the Effect of Ammonium
1013   on Aerosol Droplet pH, Environmental Science & Technology, 10.1021/acs.est.0c07394, 2020.

1014   Huffman, J. A., Perring, A. E., Savage, N. J., Clot, B., Crouzy, B., Tummon, F., Shoshanim, O., Damit,
1015   B., Schneider, J., Sivaprakasam, V., Zawadowicz, M. A., Crawford, I., Gallagher, M., Topping,
1016   D., Doughty, D. C., Hill, S. C., and Pan, Y.: Real-time sensing of bioaerosols: Review and
1017   current perspectives, Aerosol Science and Technology, 54, 465-495,
1018   10.1080/02786826.2019.1664724, 2020.

1019   Ivleva, N. P., Messerer, A., Yang, X., Niessner, R., and Pöschl, U.: Raman Microspectroscopic Analysis
1020   of Changes in the Chemical Structure and Reactivity of Soot in a Diesel Exhaust Aftertreatment

1021   Model System, Environmental Science & Technology, 41, 3702-3707, 10.1021/es0612448,

1022   2007.

1023 Jacobs, M. I., Davies, J. F., Lee, L., Davis, R. D., Houle, F., and Wilson, K. R.: Exploring Chemistry in

1024   Microcompartments Using Guided Droplet Collisions in a Branched Quadrupole Trap Coupled

1025   to a Single Droplet, Paper Spray Mass Spectrometer, Analytical Chemistry, 89, 12511-12519,

1026   10.1021/acs.analchem.7b03704, 2017.

1027 Jarvis, R. M., Law, N., Shadi, I. T., O'Brien, P., Lloyd, J. R., and Goodacre, R.: Surface-Enhanced Raman

1028   Scattering from Intracellular and Extracellular Bacterial Locations, Analytical Chemistry, 80,

1029   6741-6746, 10.1021/ac800838v, 2008.

1030 Jones, R. R., Hooper, D. C., Zhang, L., Wolverson, D., and Valev, V. K.: Raman techniques:

1031   Fundamentals and frontiers, Nanoscale research letters, 14, 1-34, 2019.

1032 Jones, S. H., Friederich, P., and Donaldson, D. J.: Photochemical Aging of Levitated Aqueous Brown

1033   Carbon   Droplets,   ACS   Earth   and   Space   Chemistry,   5,   749-754,

1034   10.1021/acsearthspacechem.1c00005, 2021.

1035 Kampf, C. J., Liu, F., Reinmuth-Selzle, K., Berkemeier, T., Meusel, H., Shiraiwa, M., and Pöschl, U.:

1036   Protein Cross-Linking and Oligomerization through Dityrosine Formation upon Exposure to

1037   Ozone, Environmental Science & Technology, 49, 10859-10866, 10.1021/acs.est.5b02902,

1038   2015.

1039 Kang, E., Root, M. J., Toohey, D. W., and Brune, W. H.: Introducing the concept of Potential Aerosol

1040   Mass (PAM), Atmos. Chem. Phys., 7, 5727-5744, 10.5194/acp-7-5727-2007, 2007.

1041 Keller, A., and Burtscher, H.: A continuous photo-oxidation flow reactor for a defined measurement of

1042   the SOA formation potential of wood burning emissions, Journal of aerosol science, 49, 9-20,

1043   2012.

1044 Kerminen, V.-M., Chen, X., Vakkari, V., Petäjä, T., Kulmala, M., and Bianchi, F.: Atmospheric new

1045   particle formation and growth: review of field observations, Environmental Research Letters,

1046   13, 103003, 2018.

1047 King, M. D., Thompson, K. C., and Ward, A. D.: Laser tweezers Raman study of optically trapped aerosol

1048   droplets of seawater and oleic acid reacting with ozone: implications for cloud-droplet

1049   properties, Journal of the American chemical society, 126, 16710-16711, 2004.

1050 King, M. D., Thompson, K. C., Ward, A. D., Pfrang, C., and Hughes, B. R.: Oxidation of biogenic and

Atmospheric
Chemistry
and Physics
Discussions

1051   water-soluble compounds in aqueous and organic aerosol droplets by ozone: a kinetic and

1052   product analysis approach using laser Raman tweezers, Faraday Discussions, 137, 173-192,

1053   10.1039/B702199B, 2008.

1054   Kirkby, J., Curtius, J., Almeida, J., Dunne, E., Duplissy, J., Ehrhart, S., Franchin, A., Gagné, S., Ickes,

1055   L., and Kürten, A.: Role of sulphuric acid, ammonia and galactic cosmic rays in atmospheric

1056   aerosol nucleation, Nature, 476, 429-433, 2011.

1057   Kline, N. J., and Treado, P. J.: Raman chemical imaging of breast tissue, Journal of Raman Spectroscopy,

1058   28, 119-124, 1997.

1059   Knopf, D., Koop, T., Luo, B., Weers, U., and Peter, T.: Homogeneous nucleation of NAD and NAT in

1060   liquid stratospheric aerosols: insufficient to explain denitrification, 2002.

1061   Knopf, D. A., Luo, B. P., Krieger, U. K., and Koop, T.: Thermodynamic Dissociation Constant of the

1062   Bisulfate Ion from Raman and Ion Interaction Modeling Studies of Aqueous Sulfuric Acid at

1063   Low Temperatures, The Journal of Physical Chemistry A, 107, 4322-4332, 10.1021/jp027775+,

1064   2003.

1065   Krieger, U. K., Marcolli, C., and Reid, J. P.: Exploring the complexity of aerosol particle properties and

1066   processes using single particle techniques, Chemical Society Reviews, 41, 6631-6662, 2012.

1067   Kunihisa, R., Iwata, A., Gen, M., Chan, C. K., and Matsuki, A.: Application of SERS on the chemical

1068   speciation of individual Aitken mode particles after condensational growth, Aerosol Science

1069   and Technology, 54, 826-836, 10.1080/02786826.2020.1730298, 2020.

1070   Kuwata, M., and Martin, S. T.: Phase of atmospheric secondary organic material affects its reactivity,

1071   Proc Natl Acad Sci U S A, 109, 17354-17359, 10.1073/pnas.1209071109, 2012.

1072   Kwamena, N. O. A., Buajarern, J., and Reid, J. P.: Equilibrium Morphology of Mixed

1073   Organic/Inorganic/Aqueous Aerosol Droplets: Investigating the Effect of Relative Humidity

1074   and Surfactants, The Journal of Physical Chemistry A, 114, 5787-5795, 10.1021/jp1003648,

1075   2010.

1076   Lam, H. K., Xu, R., Choczynski, J., Davies, J. F., Ham, D., Song, M., Zuend, A., Li, W., Tse, Y. L. S.,

1077   and Chan, M. N.: Effects of liquid–liquid phase separation and relative humidity on the

1078   heterogeneous OH oxidation of inorganic–organic aerosols: insights from methylglutaric acid

1079   and ammonium sulfate particles, Atmos. Chem. Phys., 21, 2053-2066, 10.5194/acp-21-2053-

1080   2021, 2021.

1081   Laskin, A., Laskin, J., and Nizkorodov, S. A.: Chemistry of atmospheric brown carbon, Chem Rev, 115,

1082   4335-4382, 10.1021/cr5006167, 2015.

1083   Laskina, O., Young, M. A., Kleiber, P. D., and Grassian, V. H.: Infrared extinction spectroscopy and

1084   micro-Raman spectroscopy of select components of mineral dust mixed with organic

1085   compounds, Journal of Geophysical Research: Atmospheres, 118, 6593-6606,

1086   https://doi.org/10.1002/jgrd.50494, 2013.

1087   Laucks, M. L., Roll, G., Schweiger, G., and Davis, E. J.: PHYSICAL AND CHEMICAL (RAMAN)

1088   CHARACTERIZATION OF BIOAEROSOLS—POLLEN, Journal of Aerosol Science, 31,

1089   307-319, https://doi.org/10.1016/S0021-8502(99)00058-0, 2000.

1090   Lee, A. K., Ling, T., and Chan, C. K.: Understanding hygroscopic growth and phase transformation of

1091   aerosols using single particle Raman spectroscopy in an electrodynamic balance, Faraday

1092   Discussions, 137, 245-263, 2008a.

1093   Lee, A. K. Y., and Chan, C. K.: Single particle Raman spectroscopy for investigating atmospheric

1094   heterogeneous reactions of organic aerosols, Atmospheric Environment, 41, 4611-4621,

1095   https://doi.org/10.1016/j.atmosenv.2007.03.040, 2007a.

1096   Lee, A. K. Y., and Chan, C. K.: Heterogeneous Reactions of Linoleic Acid and Linolenic Acid Particles

1097   with Ozone: Reaction Pathways and Changes in Particle Mass, Hygroscopicity, and

1098   Morphology, The Journal of Physical Chemistry A, 111, 6285-6295, 10.1021/jp071812l, 2007b.

1099   Lee, A. K. Y., Li, Y. J., Lau, A. P. S., and Chan, C. K.: A Re-Evaluation on the Atmospheric Significance

1100   of Octanal Vapor Uptake by Acidic Particles: Roles of Particle Acidity and Gas-Phase Octanal

1101   Concentration, Aerosol Science and Technology, 42, 992-1000, 10.1080/02786820802382736,

1102   2008b.

1103   Lee, J. S., Ahn, Y., Kim, J., Kim, J., Nam, S. H., Yu, S.-C., Shin, H. H., Jung, T., Kim, E.-A., Suh, Y. D.,

1104   Kim, H. W., and Park, H.-R.: Chemical analysis of air pollutant particulate matters based on

1105   surface enhanced Raman spectroscopy (SERS), SPIE Nanoscience + Engineering, SPIE, 2019.

1106   Li, J. F., Huang, Y. F., Ding, Y., Yang, Z. L., Li, S. B., Zhou, X. S., Fan, F. R., Zhang, W., Zhou, Z. Y.,

1107   Wu, D. Y., Ren, B., Wang, Z. L., and Tian, Z. Q.: Shell-isolated nanoparticle-enhanced Raman

1108   spectroscopy, Nature, 464, 392-395, 10.1038/nature08907, 2010.

1109   Li, Y. J., Lee, A. K., Lau, A. P., and Chan, C. K.: Accretion reactions of octanal catalyzed by sulfuric acid:

1110   Product identification, reaction pathways, and atmospheric implications, Environmental science

1111   & technology, 42, 7138-7145, 2008.

1112   Liang, Z., Zhang, R., Gen, M., Chu, Y., and Chan, C. K.: Nitrate Photolysis in Mixed Sucrose–Nitrate–

1113   Sulfate Particles at Different Relative Humidities, The Journal of Physical Chemistry A,

1114   10.1021/acs.jpca.1c00669, 2021.

1115   Ling, T. Y., and Chan, C. K.: Formation and Transformation of Metastable Double Salts from the

1116   Crystallization of Mixed Ammonium Nitrate and Ammonium Sulfate Particles, Environmental

1117   Science & Technology, 41, 8077-8083, 10.1021/es071419t, 2007.

1118   Ling, T. Y., and Chan, C. K.: Partial crystallization and deliquescence of particles containing ammonium

1119   sulfate and dicarboxylic acids, Journal of Geophysical Research: Atmospheres, 113,

1120   https://doi.org/10.1029/2008JD009779, 2008.

1121   Liu, X., Knauer, M., Ivleva, N. P., Niessner, R., and Haisch, C.: Synthesis of Core−Shell Surface-

1122   Enhanced Raman Tags for Bioimaging, Analytical Chemistry, 82, 441-446, 10.1021/ac902573p,

1123   2010.

1124   Liu, Y., Zhu, T., Zhao, D., and Zhang, Z.: Investigation of the hygroscopic properties of Ca (NO 3) 2 and

1125   internally mixed Ca (NO 3) 2/CaCO 3 particles by micro-Raman spectrometry, 2008.

1126   Liu, Y., Zhou, H., Hu, Z., Yu, G., Yang, D., and Zhao, J.: Label and label-free based surface-enhanced

1127   Raman scattering for pathogen bacteria detection: A review, Biosensors and Bioelectronics, 94,

1128   131-140, https://doi.org/10.1016/j.bios.2017.02.032, 2017.

1129   Liu, Y., Wang, T., Fang, X., Deng, Y., Cheng, H., Bacha, A.-U.-R., Nabi, I., and Zhang, L.: Brown carbon:

1130   An underlying driving force for rapid atmospheric sulfate formation and haze event, Science of

1131   The Total Environment, 734, 139415, https://doi.org/10.1016/j.scitotenv.2020.139415, 2020.

1132   Mabato, B. R. G., Gen, M., Chu, Y., and Chan, C. K.: Reactive Uptake of Glyoxal by Methylaminium-

1133   Containing Salts as a Function of Relative Humidity, ACS Earth and Space Chemistry, 3, 150-

1134   157, 10.1021/acsearthspacechem.8b00154, 2019.

1135   Mael, L. E., Busse, H., and Grassian, V. H.: Measurements of Immersion Freezing and Heterogeneous

1136   Chemistry of Atmospherically Relevant Single Particles with Micro-Raman Spectroscopy,

1137   Analytical Chemistry, 91, 11138-11145, 10.1021/acs.analchem.9b01819, 2019.

1138   Mekic, M., Wang, Y., Loisel, G., Vione, D., and Gligorovski, S.: Ionic Strength Effect Alters the

1139   Heterogeneous Ozone Oxidation of Methoxyphenols in Going from Cloud Droplets to Aerosol

1140   Deliquescent Particles, Environmental Science & Technology, 54, 12898-12907,

1141   10.1021/acs.est.0c03648, 2020.

1142   Meresman, H., Wills, J. B., Summers, M., McGloin, D., and Reid, J. P.: Manipulation and
1143   characterisation of accumulation and coarse mode aerosol particles using a Bessel beam trap,
1144   Physical Chemistry Chemical Physics, 11, 11333-11339, 2009.

1145   Mikhailov, E., Vlasenko, S., Martin, S. T., Koop, T., and Pöschl, U.: Amorphous and crystalline aerosol
1146   particles interacting with water vapor: conceptual framework and experimental evidence for
1147   restructuring, phase transitions and kinetic limitations, Atmos. Chem. Phys., 9, 9491-9522,
1148   10.5194/acp-9-9491-2009, 2009.

1149   Mitchem, L., Buajarern, J., Hopkins, R. J., Ward, A. D., Gilham, R. J. J., Johnston, R. L., and Reid, J. P.:
1150   Spectroscopy of Growing and Evaporating Water Droplets: Exploring the Variation in
1151   Equilibrium Droplet Size with Relative Humidity, The Journal of Physical Chemistry A, 110,
1152   8116-8125, 10.1021/jp061135f, 2006.

1153   Mitchem, L., and Reid, J. P.: Optical manipulation and characterisation of aerosol particles using a single-
1154   beam gradient force optical trap, Chemical Society Reviews, 37, 756-769, 10.1039/B609713H,
1155   2008.

1156   Mosier-Boss, P. A.: Review on SERS of Bacteria, Biosensors, 7, 51, 2017.

1157   Movasaghi, Z., Rehman, S., and Rehman, I. U.: Raman Spectroscopy of Biological Tissues, Applied
1158   Spectroscopy Reviews, 42, 493-541, 10.1080/05704920701551530, 2007.

1159   Nishikida, K., Nishio, E., and Hannah, R. W.: Selected applications of modern FT-IR techniques,
1160   Routledge, 2018.

1161   Offroy, M., Moreau, M., Sobanska, S., Milanfar, P., and Duponchel, L.: Pushing back the limits of Raman
1162   imaging by coupling super-resolution and chemometrics for aerosols characterization,
1163   Scientific Reports, 5, 12303, 10.1038/srep12303, 2015.

1164   Ofner, J., Deckert-Gaudig, T., Kamilli, K. A., Held, A., Lohninger, H., Deckert, V., and Lendl, B.: Tip-
1165   Enhanced Raman Spectroscopy of Atmospherically Relevant Aerosol Nanoparticles, Analytical
1166   Chemistry, 88, 9766-9772, 10.1021/acs.analchem.6b02760, 2016.

1167   Olson, N. E., Lei, Z., Craig, R. L., Zhang, Y., Chen, Y., Lambe, A. T., Zhang, Z., Gold, A., Surratt, J. D.,
1168   and Ault, A. P.: Reactive Uptake of Isoprene Epoxydiols Increases the Viscosity of the Core of
1169   Phase-Separated Aerosol Particles, ACS Earth and Space Chemistry, 3, 1402-1414,
1170   10.1021/acsearthspacechem.9b00138, 2019.

Atmospheric
Chemistry
and Physics
Discussions

1171 Parsons, M. T., Mak, J., Lipetz, S. R., and Bertram, A. K.: Deliquescence of malonic, succinic, glutaric,

1172   and adipic acid particles, Journal of Geophysical Research: Atmospheres, 109,

1173   https://doi.org/10.1029/2003JD004075, 2004.

1174 Peng, C., Chan, M. N., and Chan, C. K.: The Hygroscopic Properties of Dicarboxylic and Multifunctional

1175   Acids: Measurements and UNIFAC Predictions, Environmental Science & Technology, 35,

1176   4495-4501, 10.1021/es0107531, 2001.

1177 Pöschl, U.: Atmospheric Aerosols: Composition, Transformation, Climate and Health Effects,

1178   Angewandte Chemie International Edition, 44, 7520-7540,

1179   https://doi.org/10.1002/anie.200501122, 2005.

1180 Power, R., Simpson, S., Reid, J., and Hudson, A.: The transition from liquid to solid-like behaviour in

1181   ultrahigh viscosity aerosol particles, Chemical Science, 4, 2597-2604, 2013.

1182 Price, C. L., Bain, A., Wallace, B. J., Preston, T. C., and Davies, J. F.: Simultaneous Retrieval of the Size

1183   and Refractive Index of Suspended Droplets in a Linear Quadrupole Electrodynamic Balance,

1184   The Journal of Physical Chemistry A, 124, 1811-1820, 10.1021/acs.jpca.9b10748, 2020.

1185 Qiu, J., Ishizuka, S., Tonokura, K., and Enami, S.: Interfacial vs Bulk Ozonolysis of Nerolidol,

1186   Environmental Science & Technology, 53, 5750-5757, 10.1021/acs.est.9b00364, 2019.

1187 Qiu, J., Liang, Z., Tonokura, K., Colussi, A. J., and Enami, S.: Stability of Monoterpene-Derived α-

1188   Hydroxyalkyl-Hydroperoxides in Aqueous Organic Media: Relevance to the Fate of

1189   Hydroperoxides in Aerosol Particle Phases, Environmental Science & Technology, 54, 3890-

1190   3899, 10.1021/acs.est.9b07497, 2020.

1191 Radić, N., and Prkić, A.: Historical remarks on the Henderson-Hasselbalch equation: its advantages and

1192   limitations and a novel approach for exact pH calculation in buffer region, Reviews in

1193   Analytical Chemistry, 31, 93-98, 2012.

1194 Redding, B., Schwab, M. J., and Pan, Y.-l.: Raman spectroscopy of optically trapped single biological

1195   micro-particles, Sensors, 15, 19021-19046, 2015.

1196 Reid, J. P., and Mitchem, L.: LASER PROBING OF SINGLE-AEROSOL DROPLET DYNAMICS,

1197   Annual Review of Physical Chemistry, 57, 245-271,

1198   10.1146/annurev.physchem.57.032905.104621, 2006.

1199 Richards, D. S., Trobaugh, K. L., Hajek-Herrera, J., Price, C. L., Sheldon, C. S., Davies, J. F., and Davis,

1200   R. D.: Ion-molecule interactions enable unexpected phase transitions in organic-inorganic

1201   aerosol, Science Advances, 6, eabb5643, 10.1126/sciadv.abb5643, 2020.

1202   Rindelaub, J. D., Craig, R. L., Nandy, L., Bondy, A. L., Dutcher, C. S., Shepson, P. B., and Ault, A. P.:

1203   Direct Measurement of pH in Individual Particles via Raman Microspectroscopy and Variation

1204   in Acidity with Relative Humidity, The Journal of Physical Chemistry A, 120, 911-917,

1205   10.1021/acs.jpca.5b12699, 2016.

1206   Rkiouak, L., Tang, M., Camp, J., McGregor, J., Watson, I., Cox, R., Kalberer, M., Ward, A., and Pope,

1207   F.: Optical trapping and Raman spectroscopy of solid particles, Physical Chemistry Chemical

1208   Physics, 16, 11426-11434, 2014.

1209   Rodriguez, R. D., Sheremet, E., Deckert-Gaudig, T., Chaneac, C., Hietschold, M., Deckert, V., and Zahn,

1210   D. R. T.: Surface- and tip-enhanced Raman spectroscopy reveals spin-waves in iron oxide

1211   nanoparticles, Nanoscale, 7, 9545-9551, 10.1039/C5NR01277E, 2015.

1212   Roy, P., Mael, L. E., Makhnenko, I., Martz, R., Grassian, V. H., and Dutcher, C. S.: Temperature-

1213   Dependent Phase Transitions of Aqueous Aerosol Droplet Systems in Microfluidic Traps, ACS

1214   Earth and Space Chemistry, 4, 1527-1539, 10.1021/acsearthspacechem.0c00114, 2020.

1215   Rygula, A., Majzner, K., Marzec, K. M., Kaczor, A., Pilarczyk, M., and Baranska, M.: Raman

1216   spectroscopy of proteins: a review, Journal of Raman Spectroscopy, 44, 1061-1076, 2013.

1217   Sahoo, S. K., Umapathy, S., and Parker, A. W.: Time-Resolved Resonance Raman Spectroscopy:

1218   Exploring Reactive Intermediates, Applied Spectroscopy, 65, 1087-1115, 2011.

1219   Saniel, M. B. B., Lim, L. H. V., and Lamorena, R. B.: An Initial Study on the Feasibility of Using

1220   Rudimentary SERS in Quick Chemical Assessment of Ambient Aerosols, ChemistrySelect, 4,

1221   14082-14090, https://doi.org/10.1002/slct.201903479, 2019.

1222   Sauerwein, M., and Chan, C. K.: Heterogeneous uptake of ammonia and dimethylamine into sulfuric and

1223   oxalic acid particles, Atmospheric Chemistry & Physics, 17, 2017.

1224   Schill, G. P., De Haan, D. O., and Tolbert, M. A.: Heterogeneous Ice Nucleation on Simulated Secondary

1225   Organic Aerosol, Environmental Science & Technology, 48, 1675-1682, 10.1021/es4046428,

1226   2014.

1227   Scolaro, S., Sobanska, S., Barbillat, J., Laureyns, J., Louis, F., Petitprez, D., and Brémard, C.: Confocal

1228   Raman imaging and atomic force microscopy of the surface reaction of NO2 and NaCl(100)

1229   under humidity, Journal of Raman Spectroscopy, 40, 157-163, https://doi.org/10.1002/jrs.2098,

1230   2009a.

1231   Scolaro, S., Sobanska, S., Barbillat, J., Laureyns, J., Louis, F., Petitprez, D., and Brémard, C.: Confocal

1232   Raman imaging and atomic force microscopy of the surface reaction of NO2 and NaCl (100)

1233   under humidity, Journal of Raman Spectroscopy: An International Journal for Original Work in

1234   all Aspects of Raman Spectroscopy, Including Higher Order Processes, and also Brillouin and

1235   Rayleigh Scattering, 40, 157-163, 2009b.

1236   Seinfeld, J. H., and Pandis, S. N.: Atmospheric chemistry and physics: from air pollution to climate

1237   change, John Wiley & Sons, 2016.

1238   Seng, S., Guo, F., Tobon, Y. A., Ishikawa, T., Moreau, M., Ishizaka, S., and Sobanska, S.: Deliquescence

1239   behavior of photo-irradiated single NaNO3 droplets, Atmospheric Environment, 183, 33-39,

1240   https://doi.org/10.1016/j.atmosenv.2018.04.007, 2018.

1241   Sengupta, A., Laucks, M. L., Dildine, N., Drapala, E., and Davis, E. J.: Bioaerosol characterization by

1242   surface-enhanced Raman spectroscopy (SERS), Journal of Aerosol Science, 36, 651-664,

1243   https://doi.org/10.1016/j.jaerosci.2004.11.001, 2005.

1244   Setschenow, J.: Über die Konstitution der Salzlösungen auf Grund ihres Verhaltens zu Kohlensäure,

1245   Zeitschrift für Physikalische Chemie, 4U, 117, https://doi.org/10.1515/zpch-1889-0409, 1889.

1246   Sivaprakasam, V., Hart, M. B., and Eversole, J. D.: Surface Enhanced Raman Spectroscopy of Individual

1247   Suspended Aerosol Particles, The Journal of Physical Chemistry C, 121, 22326-22334,

1248   10.1021/acs.jpcc.7b05310, 2017.

1249   Sivaprakasam, V., and Hart, M. B.: Surface-Enhanced Raman Spectroscopy for Environmental

1250   Monitoring of Aerosols, ACS Omega, 10.1021/acsomega.1c00207, 2021.

1251   Smith, J., Kroll, J., Cappa, C., Che, D., Liu, C., Ahmed, M., Leone, S., Worsnop, D., and Wilson, K.: The

1252   heterogeneous reaction of hydroxyl radicals with sub-micron squalane particles: a model system

1253   for understanding the oxidative aging of ambient aerosols, Atmospheric Chemistry and Physics,

1254   9, 3209-3222, 2009.

1255   Sobanska, S., Falgayrac, G., Laureyns, J., and Brémard, C.: Chemistry at level of individual aerosol

1256   particle using multivariate curve resolution of confocal Raman image, Spectrochimica Acta Part

1257   A: Molecular   and   Biomolecular   Spectroscopy,   64,   1102-1109,

1258   https://doi.org/10.1016/j.saa.2005.11.038, 2006.

1259   Sobanska, S., Falgayrac, G., Rimetz-Planchon, J., Perdrix, E., Brémard, C., and Barbillat, J.: Resolving

1260   the internal structure of individual atmospheric aerosol particle by the combination of Atomic

1261   Force Microscopy, ESEM–EDX, Raman and ToF–SIMS imaging, Microchemical Journal, 114,

1262   89-98, https://doi.org/10.1016/j.microc.2013.12.007, 2014.

1263 Sobanska, S., Dappe, V., Siepka, D., Moreau, M., Tobon, Y., and Stefaniak, E. A.: Automated Raman

1264   microspectrometry and Raman imaging for atmospheric particle, Euroanalysis 2015, Bordeaux,

1265   France, 2015-09, 2015.

1266 Socrates, G.: Infrared and Raman characteristic group frequencies: tables and charts, John Wiley & Sons,

1267   2004.

1268 Song, M., Marcolli, C., Krieger, U., Zuend, A., and Peter, T.: Liquid-liquid phase separation and

1269   morphology of internally mixed dicarboxylic acids/ammonium sulfate/water particles,

1270   Atmospheric Chemistry and Physics, 12, 2691-2712, 2012a.

1271 Song, M., Marcolli, C., Krieger, U., Zuend, A., and Peter, T.: Liquid-liquid phase separation in aerosol

1272   particles: Dependence on O: C, organic functionalities, and compositional complexity,

1273   Geophysical research letters, 39, 2012b.

1274 Song, M., Marcolli, C., Krieger, U. K., Lienhard, D. M., and Peter, T.: Morphologies of mixed

1275   organic/inorganic/aqueous aerosol droplets, Faraday discussions, 165, 289-316, 2013.

1276 Steer, B., Gorbunov, B., Price, M. C., and Podoleanu, A.: Raman spectroscopic identification of size-

1277   selected airborne particles for quantitative exposure assessment, Measurement Science and

1278   Technology, 27, 045801, 2016.

1279 Su, H., Cheng, Y., and Pöschl, U.: New Multiphase Chemical Processes Influencing Atmospheric

1280   Aerosols, Air Quality, and Climate in the Anthropocene, Accounts of Chemical Research, 53,

1281   2034-2043, 10.1021/acs.accounts.0c00246, 2020.

1282 Sun, Z., Duan, F., He, K., Du, J., Yang, L., Li, H., Ma, T., and Yang, S.: Physicochemical analysis of

1283   individual atmospheric fine particles based on effective surface-enhanced Raman spectroscopy,

1284   Journal of Environmental Sciences, 75, 388-395, https://doi.org/10.1016/j.jes.2018.06.006,

1285   2019a.

1286 Sun, Z., Duan, F., He, K., Du, J., and Zhu, L.: Sulfate–nitrate–ammonium as double salts in PM2.5:

1287   Direct observations and implications for haze events, Science of The Total Environment, 647,

1288   204-209, https://doi.org/10.1016/j.scitotenv.2018.07.107, 2019b.

1289 Tahir, M. A., Zhang, X., Cheng, H., Xu, D., Feng, Y., Sui, G., Fu, H., Valev, V. K., Zhang, L., and Chen,

1290   J.: Klarite as a label-free SERS-based assay: a promising approach for atmospheric bioaerosol

1291   detection, Analyst, 145, 277-285, 10.1039/C9AN01715A, 2020.

1292 Talari, A. C. S., Movasaghi, Z., Rehman, S., and Rehman, I. U.: Raman spectroscopy of biological tissues,

1293   Applied spectroscopy reviews, 50, 46-111, 2015.

1294 Tang, M., Chan, C. K., Li, Y. J., Su, H., Ma, Q., Wu, Z., Zhang, G., Wang, Z., Ge, M., Hu, M., He, H.,

1295   and Wang, X.: A review of experimental techniques for aerosol hygroscopicity studies, Atmos.

1296   Chem. Phys., 19, 12631-12686, 10.5194/acp-19-12631-2019, 2019.

1297 Tang, M. J., Camp, J. C. J., Rkiouak, L., McGregor, J., Watson, I. M., Cox, R. A., Kalberer, M., Ward, A.

1298   D., and Pope, F. D.: Heterogeneous Interaction of SiO2 with N2O5: Aerosol Flow Tube and

1299   Single Particle Optical Levitation–Raman Spectroscopy Studies, The Journal of Physical

1300   Chemistry A, 118, 8817-8827, 10.1021/jp506753c, 2014.

1301 Tirella, P. N., Craig, R. L., Tubbs, D. B., Olson, N. E., Lei, Z., and Ault, A. P.: Extending surface enhanced

1302   Raman spectroscopy (SERS) of atmospheric aerosol particles to the accumulation mode (150–

1303   800 nm), Environmental Science: Processes & Impacts, 20, 1570-1580, 10.1039/C8EM00276B,

1304   2018.

1305 Tobon, Y. A., Seng, S., Picone, L. A., Bava, Y. B., Juncal, L. C., Moreau, M., Romano, R. M., Barbillat,

1306   J., and Sobanska, S.: Photochemistry of single particles using acoustic levitation coupled with

1307   Raman microspectrometry, Journal of Raman Spectroscopy, 48, 1135-1137,

1308   https://doi.org/10.1002/jrs.5181, 2017.

1309 Tolles, W. M., Nibler, J., McDonald, J., and Harvey, A.: A review of the theory and application of

1310   coherent anti-Stokes Raman spectroscopy (CARS), Applied Spectroscopy, 31, 253-271, 1977.

1311 Treuel, L., Pederzani, S., and Zellner, R.: Deliquescence behaviour and crystallisation of ternary

1312   ammonium sulfate/dicarboxylic acid/water aerosols, Physical Chemistry Chemical Physics, 11,

1313   7976-7984, 10.1039/B905007H, 2009.

1314 Tripathi, A., Jabbour, R. E., Guicheteau, J. A., Christesen, S. D., Emge, D. K., Fountain, A. W., Bottiger,

1315   J. R., Emmons, E. D., and Snyder, A. P.: Bioaerosol Analysis with Raman Chemical Imaging

1316   Microspectroscopy, Analytical Chemistry, 81, 6981-6990, 10.1021/ac901074c, 2009.

1317 Tsai, J.-H. M., Harrison, J. G., Martin, J. C., Hamilton, T. P., van der Woerd, M., Jablonsky, M. J., and

1318   Beckman, J. S.: Role of Conformation of Peroxynitrite Anion (ONOO-) with Its Stability and

1319   Toxicity, Journal of the American Chemical Society, 116, 4115-4116, 10.1021/ja00088a072,

1320   1994.

1321 Vejpongsa, I., Suvachittanont, S., Klinklan, N., Thongyen, T., Veres, M., and Szymanski, W. W.:
1322   Deliberation between PM1 and PM2.5 as air quality indicators based on comprehensive
1323   characterization of urban aerosols in Bangkok, Thailand, Particuology, 35, 1-9,
1324   https://doi.org/10.1016/j.partic.2017.05.001, 2017.

1325 Wang, C., Pan, Y.-L., Hill, S. C., and Redding, B.: Photophoretic trapping-Raman spectroscopy for single
1326   pollens and fungal spores trapped in air, Journal of Quantitative Spectroscopy and Radiative
1327   Transfer, 153, 4-12, 2015a.

1328 Wang, Y., Ma, J.-B., Zhou, Q., Pang, S.-F., and Zhang, Y.-H.: Hygroscopicity of Mixed
1329   Glycerol/Mg(NO3)2/Water Droplets Affected by the Interaction between Magnesium Ions and
1330   Glycerol Molecules, The Journal of Physical Chemistry B, 119, 5558-5566,
1331   10.1021/acs.jpcb.5b00458, 2015b.

1332 Wei, H., Vejerano, E. P., Leng, W., Huang, Q., Willner, M. R., Marr, L. C., and Vikesland, P. J.: Aerosol
1333   microdroplets exhibit a stable pH gradient, Proceedings of the National Academy of Sciences,
1334   115, 7272-7277, 10.1073/pnas.1720488115, 2018a.

1335 Wei, H., Vejerano, E. P., Leng, W., Huang, Q., Willner, M. R., Marr, L. C., and Vikesland, P. J.: Aerosol
1336   microdroplets exhibit a stable pH gradient, Proceedings of the National Academy of Sciences,
1337   115, 7272, 10.1073/pnas.1720488115, 2018b.

1338 Wheeler, M. J., Mason, R. H., Steunenberg, K., Wagstaff, M., Chou, C., and Bertram, A. K.: Immersion
1339   Freezing of Supermicron Mineral Dust Particles: Freezing Results, Testing Different Schemes
1340   for Describing Ice Nucleation, and Ice Nucleation Active Site Densities, The Journal of Physical
1341   Chemistry A, 119, 4358-4372, 10.1021/jp507875q, 2015.

1342 Willis, M. D., Rovelli, G., and Wilson, K. R.: Combining Mass Spectrometry of Picoliter Samples with
1343   a Multicompartment Electrodynamic Trap for Probing the Chemistry of Droplet Arrays,
1344   Analytical Chemistry, 92, 11943-11952, 10.1021/acs.analchem.0c02343, 2020.

1345 Wise, M. E., Baustian, K. J., and Tolbert, M. A.: Internally mixed sulfate and organic particles as potential
1346   ice nuclei in the tropical tropopause region, Proceedings of the National Academy of Sciences,
1347   107, 6693-6698, 2010.

1348 Wise, M. E., Baustian, K. J., Koop, T., Freedman, M. A., Jensen, E. J., and Tolbert, M. A.: Depositional
1349   ice nucleation onto crystalline hydrated NaCl particles: a new mechanism for ice formation in
1350   the troposphere, Atmospheric Chemistry and Physics, 12, 1121-1134, 2012.

Wu, H. B., Chan, M. N., and Chan, C. K.: FTIR Characterization of Polymorphic Transformation of Ammonium Nitrate, Aerosol Science and Technology, 41, 581-588, 10.1080/02786820701272038, 2007.

Wu, H. B., and Chan, C. K.: Effects of potassium nitrate on the solid phase transitions of ammonium nitrate particles, Atmospheric Environment, 42, 313-322, 2008.

Wu, Z., Wang, Y., Tan, T., Zhu, Y., Li, M., Shang, D., Wang, H., Lu, K., Guo, S., Zeng, L., and Zhang, Y.: Aerosol Liquid Water Driven by Anthropogenic Inorganic Salts: Implying Its Key Role in Haze Formation over the North China Plain, Environmental Science & Technology Letters, 5, 160-166, 10.1021/acs.estlett.8b00021, 2018.

Xu, G., Cheng, H., Jones, R., Feng, Y., Gong, K., Li, K., Fang, X., Tahir, M. A., Valev, V. K., and Zhang, L.: Surface-Enhanced Raman Spectroscopy Facilitates the Detection of Microplastics <1 μm in the Environment, Environmental Science & Technology, 54, 15594-15603, 10.1021/acs.est.0c02317, 2020a.

Xu, R., Ge, Y., Kwong, K. C., Poon, H. Y., Wilson, K. R., Yu, J. Z., and Chan, M. N.: Inorganic Sulfur Species Formed upon Heterogeneous OH Oxidation of Organosulfates: A Case Study of Methyl Sulfate, ACS Earth and Space Chemistry, 4, 2041-2049, 10.1021/acsearthspacechem.0c00209, 2020b.

Yeung, M. C., and Chan, C. K.: Water Content and Phase Transitions in Particles of Inorganic and Organic Species and their Mixtures Using Micro-Raman Spectroscopy, Aerosol Science and Technology, 44, 269-280, 10.1080/02786820903583786, 2010.

Yeung, M. C., Ling, T. Y., and Chan, C. K.: Effects of the Polymorphic Transformation of Glutaric Acid Particles on Their Deliquescence and Hygroscopic Properties, The Journal of Physical Chemistry A, 114, 898-903, 10.1021/jp908250v, 2010.

You, Y., Renbaum-Wolff, L., Carreras-Sospedra, M., Hanna, S. J., Hiranuma, N., Kamal, S., Smith, M. L., Zhang, X., Weber, R. J., Shilling, J. E., Dabdub, D., Martin, S. T., and Bertram, A. K.: Images reveal that atmospheric particles can undergo liquid–liquid phase separations, Proceedings of the National Academy of Sciences, 109, 13188, 10.1073/pnas.1206414109, 2012.

You, Y., Renbaum-Wolff, L., and Bertram, A. K.: Liquid–liquid phase separation in particles containing organics mixed with ammonium sulfate, ammonium bisulfate, ammonium nitrate or sodium chloride, Atmos. Chem. Phys., 13, 11723-11734, 10.5194/acp-13-11723-2013, 2013.

46

1381   You, Y., Smith, M. L., Song, M., Martin, S. T., and Bertram, A. K.: Liquid–liquid phase separation in
1382   atmospherically relevant particles consisting of organic species and inorganic salts,
1383   International Reviews in Physical Chemistry, 33, 43-77, 10.1080/0144235X.2014.890786,
1384   2014.

1385   Yu, J.-Y., Zhang, Y., Tan, S.-H., Liu, Y., and Zhang, Y.-H.: Observation on the Ion Association Equilibria
1386   in NaNO3 Droplets Using Micro-Raman Spectroscopy, The Journal of Physical Chemistry B,
1387   116, 12581-12589, 10.1021/jp306367v, 2012.

1388   Yu, T., Zhao, D., Song, X., and Zhu, T.: NO2-initiated multiphase oxidation of SO2 by O2 on CaCO3
1389   particles, Atmos. Chem. Phys, 18, 6679-6689, 2018.

1390   Zangmeister, C. D., and Pemberton, J. E.: Raman Spectroscopy of the Reaction of Sodium Chloride with
1391   Nitric Acid: Sodium Nitrate Growth and Effect of Water Exposure, The Journal of Physical
1392   Chemistry A, 105, 3788-3795, 10.1021/jp003374n, 2001.

1393   Zardini, A. A., Sjogren, S., Marcolli, C., Krieger, U. K., Gysel, M., Weingartner, E., Baltensperger, U.,
1394   and Peter, T.: A combined particle trap/HTDMA hygroscopicity study of mixed
1395   inorganic/organic aerosol particles, Atmos. Chem. Phys., 8, 5589-5601, 10.5194/acp-8-5589-
1396   2008, 2008.

1397   Zhang, R., Wang, G., Guo, S., Zamora, M. L., Ying, Q., Lin, Y., Wang, W., Hu, M., and Wang, Y.:
1398   Formation of urban fine particulate matter, Chemical reviews, 115, 3803-3855, 2015.

1399   Zhang, R., Gen, M., Huang, D., Li, Y., and Chan, C. K.: Enhanced Sulfate Production by Nitrate
1400   Photolysis in the Presence of Halide Ions in Atmospheric Particles, Environmental Science &
1401   Technology, 54, 3831-3839, 10.1021/acs.est.9b06445, 2020.

1402   Zhang, R., Gen, M., Fu, T.-M., and Chan, C. K.: Production of Formate via Oxidation of Glyoxal
1403   Promoted by Particulate Nitrate Photolysis, Environmental Science & Technology,
1404   10.1021/acs.est.0c08199, 2021.

1405   Zhang, Y.-H., and Chan, C. K.: Study of Contact Ion Pairs of Supersaturated Magnesium Sulfate
1406   Solutions Using Raman Scattering of Levitated Single Droplets, The Journal of Physical
1407   Chemistry A, 104, 9191-9196, 10.1021/jp0013659, 2000.

1408   Zhang, Y.-H., and Chan, C. K.: Observations of Water Monomers in Supersaturated NaClO4, LiClO4,
1409   and Mg(ClO4)2 Droplets Using Raman Spectroscopy, The Journal of Physical Chemistry A,
1410   107, 5956-5962, 10.1021/jp0271256, 2003.

1411 Zhang, Y.-H., Choi, M. Y., and Chan, C. K.: Relating Hygroscopic Properties of Magnesium Nitrate to

1412 the Formation of Contact Ion Pairs, The Journal of Physical Chemistry A, 108, 1712-1718,

1413 10.1021/jp036524d, 2004.

1414 Zhao, D., Song, X., Zhu, T., Zhang, Z., Liu, Y., and Shang, J.: Multiphase oxidation of SO2 by NO2 on

1415 CaCO3 particles, Atmospheric Chemistry and Physics, 18, 2481-2493, 10.5194/acp-18-2481-

1416 2018, 2018a.

1417 Zhao, D., Song, X., Zhu, T., Zhang, Z., Liu, Y., and Shang, J.: Multiphase oxidation of SO 2 by NO 2 on

1418 CaCO 3 particles, Atmospheric Chemistry and Physics, 18, 2481, 2018b.

1419 Zheng, G., Su, H., Wang, S., Andreae, M. O., Pöschl, U., and Cheng, Y.: Multiphase buffer theory

1420 explains contrasts in atmospheric aerosol acidity, Science, 369, 1374-1377, 2020a.

1421 Zheng, H., Song, S., Sarwar, G., Gen, M., Wang, S., Ding, D., Chang, X., Zhang, S., Xing, J., and Sun,

1422 Y.: Contribution of Particulate Nitrate Photolysis to Heterogeneous Sulfate Formation for

1423 Winter Haze in China, Environmental Science & Technology Letters, 7, 632-638, 2020b.

1424 Zheng, L., Kulkarni, P., Birch, M. E., Ashley, K., and Wei, S.: Analysis of Crystalline Silica Aerosol

1425 Using Portable Raman Spectrometry: Feasibility of Near Real-Time Measurement, Analytical

1426 Chemistry, 90, 6229-6239, 10.1021/acs.analchem.8b00830, 2018.

1427 Zhou, H., Yang, D., Ivleva, N. P., Mircescu, N. E., Niessner, R., and Haisch, C.: SERS Detection of

1428 Bacteria in Water by in Situ Coating with Ag Nanoparticles, Analytical Chemistry, 86, 1525-

1429 1533, 10.1021/ac402935p, 2014a.

1430 Zhou, H., Yang, D., Ivleva, N. P., Mircescu, N. E., Schubert, S., Niessner, R., Wieser, A., and Haisch, C.:

1431 Label-Free in Situ Discrimination of Live and Dead Bacteria by Surface-Enhanced Raman

1432 Scattering, Analytical Chemistry, 87, 6553-6561, 10.1021/acs.analchem.5b01271, 2015.

1433 Zhou, Q., Pang, S.-F., Wang, Y., Ma, J.-B., and Zhang, Y.-H.: Confocal Raman studies of the evolution

1434 of the physical state of mixed phthalic acid/ammonium sulfate aerosol droplets and the effect

1435 of substrates, The Journal of Physical Chemistry B, 118, 6198-6205, 2014b.

1436 Zhu, F., Zhou, H., Wang, X., Zhou, Y., Liu, H., Fang, C., and Fang, Y.: Raman spectroscopy and ab initio

1437 quantum chemical calculations of ion association behavior in calcium nitrate solution, Journal

1438 of Raman Spectroscopy, 49, 852-861, https://doi.org/10.1002/jrs.5349, 2018.

1439 Zobrist, B., Soonsin, V., Luo, B. P., Krieger, U. K., Marcolli, C., Peter, T., and Koop, T.: Ultra-slow water

1440 diffusion in aqueous sucrose glasses, Physical Chemistry Chemical Physics, 13, 3514-3526,
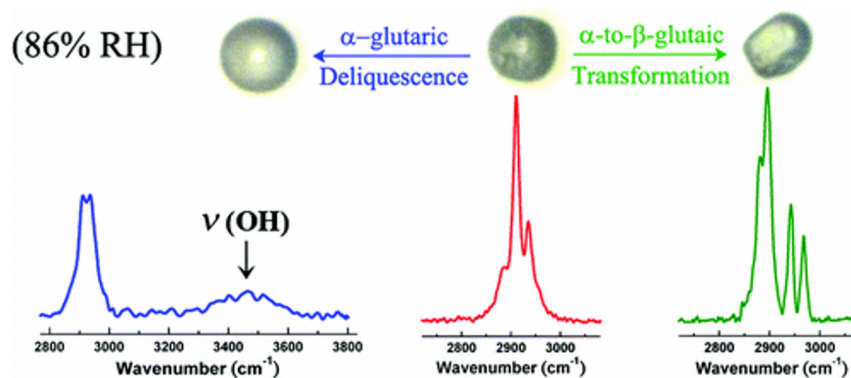
1441   2011.

1442
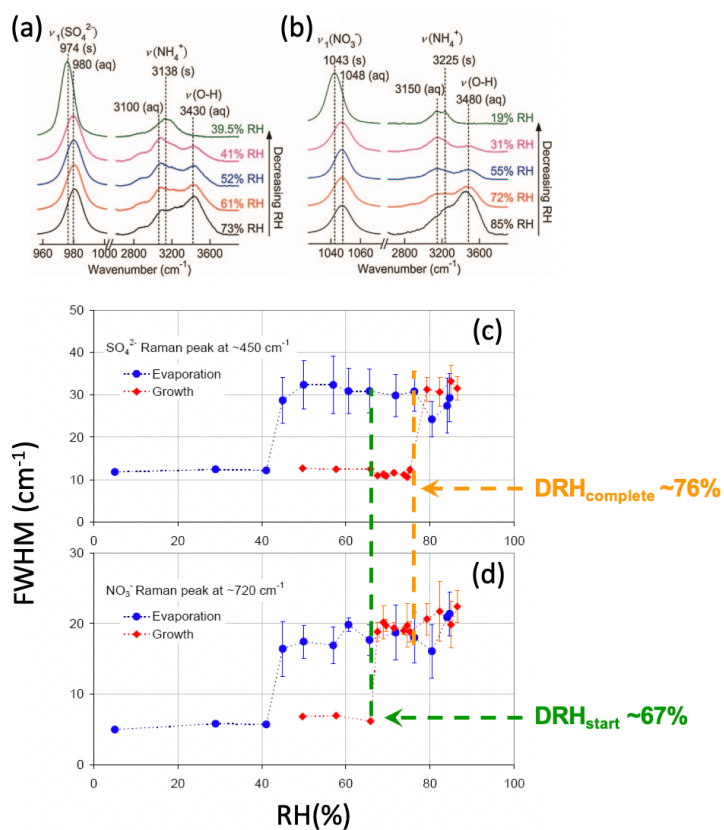
1443

1444   **Figure 1.** Raman spectra of a single (a) AS and (b) AN particle upon evaporation. FWHM of (c) SO_4^{2-}

1445   peak and (d) NO_3^- peak during the evaporation-growth cycle of a mixed AS-AN particle.

1446
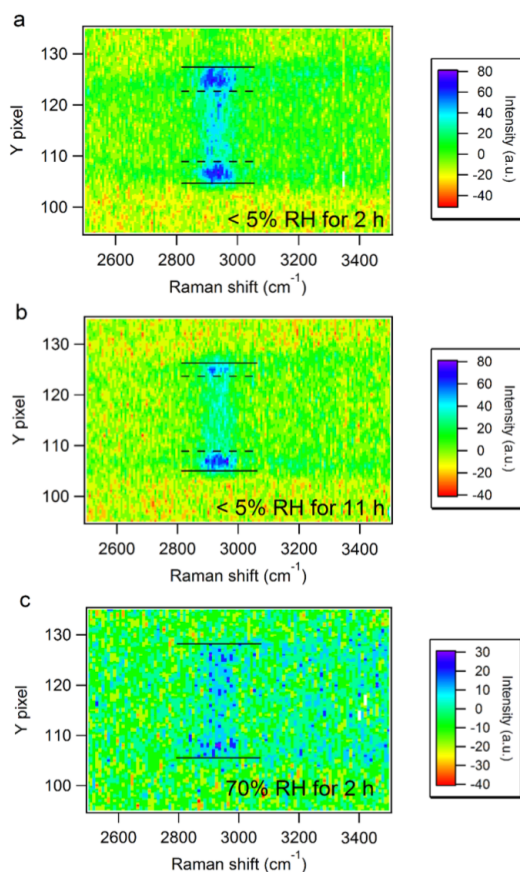

1447

1448   **Figure 2.** Raman spectra of deliquescent α-glutaric acid, crystalline α-glutaric acid and β-glutaric acid.

1449   Reprinted with permission from Yeung et al. (2010). Copyright 2010 American Chemical Society.

1450

1451

1452   **Figure 3.** Spatially resolved Raman intensities of AS – sucrose (molar fraction of sucrose in total solute

1453   (F_{SU}) = 0.5)) particles equilibrated (a) at < 5% RH for 2 hours and (b) for 11 h and (c) at 70% RH for 2

1454   hours. C-H peaks at ~2900 cm^{-1} represent sucrose. Solid lines indicate the particle's upper and lower

1455   edges. The outer regions between the dashed and solid lines are sucrose-rich in (a)-(b). Reprinted with

1456   permission by Chu and Chan. (2017a). Copyright 2017 American Chemical Society.
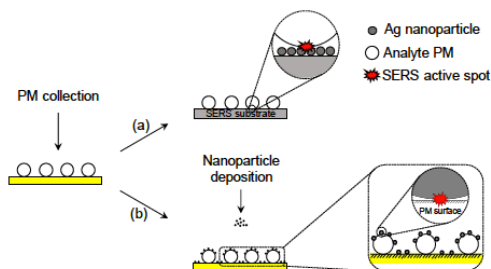
1457

Atmospheric
Chemistry
and Physics
Discussions
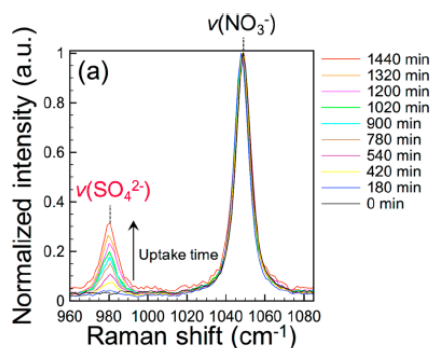
1458

1459   **Figure 4.** Sulfate formation during the photolysis of AN particles in the presence of SO_2 at 80% RH.

1460   Reprinted with permission by Gen et al. (2019b). Copyright 2019 American Chemical Society.

1461

1462

1463   **Figure 5.** Schematic illustration of (a) a conventional SERS substrate approach and (b) the ES-SERS

1464   approach. Reprinted with permission by Gen and Chan. (2017).

1465

1466   Appendix A. Major Raman peaks of atmospheric relevant species

Species		Raman shift (cm^{-1})	Ref.
Water	O-H	~3300 (monomers) ~3600 (hydrogen-bonded)	(Carey and Korenowski, 1998)
Inorganic	NH_4^+	~1413; ~1660; ~3100	(Chu and Chan, 2017a;Sauerwein and Chan, 2017)
	SO_4^{2-}	~450; ~618; ~980	(Chu and Chan, 2017a;Ling and

Atmospheric
Chemistry
and Physics
Discussions
Open Access
EGU

				Chan, 2007)
	HSO_4^-		~1053	(Rindelaub et al., 2016;Craig et al., 2017;Craig et al., 2018)
	NO_3^-		~717; ~1046; ~1413	(Gen et al., 2019b;Tobon et al., 2017)
	HNO_3		~1306	(Rindelaub et al., 2016)
	NO_2^-		~815; ~1278; ~ 1330	(Tobon et al., 2017)
	$ONOO^-$		~980	(Tobon et al., 2017;Tsai et al., 1994)
	CO_3^{2-}		~1067	(Rindelaub et al., 2016)
	HCO_3^-		~1019	(Rindelaub et al., 2016)
Soot	D		~1367	(Gen and Chan, 2017;Ivleva et al., 2007)
	G		~1585	(Gen and Chan, 2017;Ivleva et al., 2007)
Mineral dust	SiO_2	Si-O-Si	~390; ~490; ~795; ~972; ~1460	(Rkiouak et al., 2014;Laskina et al., 2013)
		O-Si-O	~356	
		Si-O	~465	
	α-Al_2O_3	Al-O-Al	~420; ~585; ~796;	(Rkiouak et al.,

Atmospheric
Chemistry
and Physics
Discussions

Open Access

EGU

		Al-OH	~976	2014)
	Kaolinite	Si-O	~397	(Laskina et al., 2013)
		Si-O-Al	~516	
		O-H	~914; 3624; 3656; 3668; 3698	
	TiO$_2$	Ti-O	~484; ~680;	Amorphous	(Rkiouak et al., 2014;Tang et al., 2014)
			~153; ~639;	Anatase	
		O-O	~250; ~317;	Amorphous	
	CaCO$_3$	CO$_3^{2-}$	~713; ~1087		(Laskina et al., 2013;Zhao et al., 2018b;Yu et al., 2018)
Organic	C-H		~1400; 2700-3000		(Chu and Chan, 2017a;Gen et al., 2018)
	C-O		~1470		(Laskina et al., 2013)
	C=O		~1700		(Yeung and Chan, 2010;Yeung et al., 2010;Bondy et al., 2018)
	O-H		~1700; 3200-3400		(Yeung and Chan, 2010;Zhou et al., 2014b)
	C-N-C		~890		(Chu and Chan, 2017a)
	O-C-O (ring)		~770		(Gen et al., 2018)
	ring		~950		(Gen et al., 2018)
	O-O		~850		(Lee and Chan,

		2007a, b)
C=C	~1600	(Lee and Chan, 2007b;Chu et al., 2019)
C=C-C=C	~1640&1655 (double peaks)	(Lee and Chan, 2007b;Chu et al., 2019)
C=C-C=O	~1690	(Chu et al., 2019;Lee and Chan, 2007b)
RO-SO$_3$	~846	(Bondy et al., 2018)
S-O (-SO$_3$ group)	1065	(Bondy et al., 2018)

1467